SSRG International Journal of Mechanical Engineering
ISSN: 2348-8360/ https://doi.org/10.14445/23488360/IJME-V12I4P108

Volume 12 Issue 4, 82-108, April 2025
© 2025 Seventh Sense Research Group®

Original Article

Optimization of Bead Geometrics for GMAW-Based Wire Arc Additive Manufacturing Using 1.36 Cr-0.5 Mo Steel Metal-Cored Wires

Prerna Shah[1, 2], Vyomesh Buch[3], Jay Vora[4]

[1]*Faculty of Engineering and Technology, Parul University, Vadodara, Gujarat, India.*
[2] *Department of Mechanical Engineering, Government Engineering College, Bharuch, Gujarat, India.*
[3]*Parul Institute of Technology, Parul University, Vadodara, Gujarat, India.*
[4]*Department of Mechanical Engineering, School of Technology, Pandit Deendayal Energy University, Gandhinagar, Gujarat, India.*

[1]*Corresponding Author : prerna..shah003@gmail.com*

Received: 09 February 2025 Revised: 07 March 2025 Accepted: 10 April 2025 Published: 30 April 2025

Abstract - *Optimizing the process parameters to achieve optimal performance of gas metal arc welding technique of wire arc additive manufacturing using Metalloy 80B2 (1.00-1.50 percent chromium and 0.50 percent molybdenum steel), a gas-shielded metal-cored wire, was the main goal of the current investigation. Depth of Penetration (DOP), bead height (BH), and Bead Width (BW) of bead deposition were examined in relation to changes in input parameters (voltage (22 to 26 V), travel speed (1 to 6 mm/s), and shielding gas composition (CO_2-1%, 5%, and 9%). Utilizing the Box Behnken Designs, the set of input variables for the experiment was determined. The significance and sufficiency of the correlation derived from the experiment's results were confirmed through the use of fit statistics and ANOVA. In contrast, to travel speed for BH, the voltage was determined to be a more significant parameter for DOP and BW. Externally studentized residual plots for DOP, BH, and BW were examined, and the results showed that created correlations are legitimate and don't require transformation. The optimum outcomes from Stat-Ease 360 software: DOP = 1.320 mm, BH = 8.381 mm, BW = 8.687 mm for voltage = 26 V, travel speed = 10 mm/s, % of CO_2 into gas mixture = 8.317% was achieved with 0.895 desirability. The experimental work for optimum input parameters was conducted and found within the range of results obtained from State Ease 360 software. Experimental results showed that the bead-on-bead material was placed uniformly in a multilayer structure, merged flawlessly, and did not disperse.*

Keywords - *Metal cored wire, Low alloy steel, Wire arc additive manufacturing, Response surface methodology, Stat-Ease 360 software.*

1. Introduction

Manufacturing technology has changed significantly throughout the years, moving from traditional manufacturing to newer technologies like additive manufacturing. Conventional manufacturing technology involves removing the material from the raw material's surface and preparing the final product through a series of machining procedures [1]. However, with additive manufacturing, numerous successive thin layers of raw material are laid down and bonded to create the final goods [2]. Three-Dimensional (3-D) printing, another name for additive manufacturing, is used to make massive, intricate structures, things with unique dimensions, etc. [3] Reduced energy consumption, energy-efficient techniques, minimal auxiliary equipment needed, lower raw waste material consumption, cost savings, and more are some advantages of additive manufacturing. The advantages of direct energy deposition over other additive manufacturing processes include the capacity to print massive structures, the ability to print functionally graded material, a high deposition, speed of deposition, and a lower total cost of manufacture. The advantages of Wire Arc Additive Manufacturing (WAAM) over other forms of direct energy deposition additive manufacturing techniques include easy handling, a safe atmosphere, lower material costs, etc. GAS TUNGSTEN ARC WELDING (GTAW), Gas Metal Arc Welding (GMAW), Double Electrode GMAW (DE-GMAW), and Cold Metal Transfer (CMT)are among the energy sources that are used to categorize the WAAM. An arc is created between the consumable electrode and the base metal workpiece in GMAW-WAAM, sometimes referred to as metal inert gas welding, which supplies filler material for the melt. Mass production can benefit from GMAW's high

This is an open access article under the CC BY-NC-ND license (http://creativecommons.org/licenses/by-nc-nd/4.0/)

deposition rate of 3 to 4 kg/h, high energy efficiency of 84%, high welding speed, high-quality welding with less spatter, ability to weld thin materials, etc. [4-7] Important process factors for the bead deposition produced with GMAW include shield gas composition, shielding gas flow rate, wire feed, wire material, voltage, torch travel speed, and torch route. The product made with the weld beads is greatly impacted by the wire type employed in GMAW, which affects dimensional accuracy, surface quality, and mechanical qualities [2, 3]. The selection criteria for wire in GMAW are based on a number of factors, including material availability, pricing, and characteristics, as well as production considerations, fabrication, service, and financial needs.

Henckel et al. [8] built layer-by-layer with alloy (aluminum-titanium, with a composition ranging from 10 to 55 percent aluminium) by varying the feeding rates utilizing hot-wire feeding in conjunction with GMAW. The micro-structural formation, a macroscopic characteristic, and the shift in the wall structure's microhardness values were all examined. Henckel et al. [9] concluded the study found by improving the geometrical and micro-structural characteristics of low-alloyed steel by reducing input energy by about 40% through the adjustment through the contact pipe to worksheet distance in the current-controlled GMAW-WAAM method. Kumar and Maji [10] developed 304L stainless steel deposited in WAAM utilizing a single-bead geometry bead created with Response Surface Methodology (RSM) and experiments carried out with Box-Behnken Design (BBD). Bead Geometry, including Width (BW), Height (BH), cross-sectional area, etc., was correlated with input parameters like wire feed rate, torch speed, voltage, and gas flow rate.

A genetic algorithm was used to identify the best deposition process conditions to reduce void and increase material yield. Bharat Kumar and Anand Krishna [11] studied the impact of WAAM input parameters on the width of the Inconel 825 material bead deposited utilizing metal inert gas welding, including welding speed, wire feed speed, and voltage. The Taguchi approach yielded the lowest BW of 3.07 mm length for the optimal parameter (welding velocity = 0.55 m/min, wire feed speed = 4 m/min, and voltage = 18 V). The authors concluded that choosing and fine-tuning the parameters reduces the weld bead's waviness, weld fractures, porosity, and discontinuity. Baby and Amirthalingam [12] studied the GMAW-WAAM process's metal transfer characteristic and how it affects microstructural assessment to suggest the best deposition method. The outcome showed that whereas long and columnar grains were seen with conventional pulsed mode deposition, the micro-structure of short-circuited pulsed mode deposition was created randomly and oriented near equiaxed grains. Pringle et al. [13] found that the most significant sensors were light and radio frequency, which demonstrated arc extinction events and a distinctive "excellent weld" peak frequency for GMAW-based 3-D printing With Aluminium Wire Feed (WAAM) for near-net form applications. Aldalur et al. [14] studied Aluminum alloy 5356, which was analyzed using the three working modes (pulsed GMAW, cold arc, and pulsed Ac) in a GMAW-based WAAM technical process. Evaluating the final products' geometrical shape and porosity levels revealed that the pulsed AC mode outperformed the other two modes. Zhao et al. [15] developed a mathematical model to predict the geometry, morphology, and heat transfer of fluids in a GMAW-based WAAM process using a wire that is 5 percent magnesium. The research results demonstrated that a droplet's maximum velocity of 0.9 m/s was seen as it dropped into a molten pool. This caused the liquid metal in the middle of the pool to flow and move towards the bottom, creating a depressed area. Additionally, the deposit profile contrasted the simulation outcomes and the experiment.

Mookara et al. [16] attempted to use CMT GMAW-based WAAM to determine the ideal deposition parameter for producing directionally solidified Inconel 625 components by using short-circuiting with pulse method for transfer of droplets. The Inconel 625 components made with short-circuiting with pulse mode displayed enhanced mechanical and corrosion-resistant qualities and a defect-free deposit with a desired microstructure. Warsi et al. [17] created Using computer numerically controlled GMAW-based WAAM, a single square bead of mild steel wire made of the low carbon alloy ER70S is placed on a warmed, normal substrate to examine the bead humping phenomenon and the control of BH's dimensional stability. The bead deposited on the warmed substrate employing WAAM showed better hardness, less humping, more dimensional stability, and less wear than the traditional approach. Vishal Kumar et al. [18] carried out an investigation to determine the ideal process parameters for the GMAW-WAAM method used to put metallic wire in a single-layer weld bead form on mild steel ER70S-6 that has been coated in copper. For the ideal process parameters, such as travel speed = 95 mm/min, open circuit voltage = 16 V, and shielding gas flowrate = 21 L/min, a single-layer bead's maximum height and minimum width were achieved.

The author researched the impact of wire feed speed, travel speed, and voltage on the BW and BH for several layers of low alloy steel beads utilizing the GMAW-WAAM process. ANOVA was used to assess the robustness and suitability of the nonlinear regression formula created between the input and output parameters. The structure was determined to be free of dis-bonding when BW = 4.73 mm and BH = 7.81 mm were obtained for the optimal input value. The author studied the impact of wire feed speed, travel speed, and voltage on BW and BH for multilayer structures produced with SS 316L metallic wire prepared using the GMAW-WAAM technique. The feasibility of the design features and performance was evaluated using variance analysis, and multi-variable regression equations were

produced. The greatest significant component influencing the BW and BH was determined to be wire feed speed. The multilayer structures showed BW = 5.01 mm and BH = 7.81 mm for the optimal input parameter. The structure was determined to be free from dis-bonding, and flawless fusing was discovered. According to the literature, the majority of the research on the WAAM method was carried out utilizing titanium alloys like Ti6Al4V [19], β-titanium alloy [20], etc., aluminium alloy such as TiC/AA7075 [21], AlMg5Mn [22], etc., and low carbon steel like 316L stainless steel, 1.25Cr-1.0Mo steel, etc. as wire material. The qualities of single and multilayer bead structures can be improved by combining different materials and alloys. Nevertheless, the literature found very little study on the WAAM technique using low-alloy steel. Additionally, the literature shows that the GMAW-WAAM process's response characteristics were examined regarding input/process variables such as voltage, travel speed, and wire feed speed; however, the effect of shielding gas composition was not noted.

The bead deposition in the current study was created utilizing a GMAW-based WAAM method on Metalloy 80B2 wire (1.00 - 1.50 percent Chromium, 0.50 percent Molybdenum), a low-alloy steel gas-shield metal-cored wire, in order to close the research gap. Response parameters like Depth Of Penetration (DOP), BH, and BW for the bead deposition made using GMAW-WAAM were examined in relation to process/input parameters like voltage (22 to 26 V), travel speed (1 to 6 mm/s), and shielding gas composition (CO_2 - 1 percent, 5 percent, and 9 percent and Argon - 99 percent, 95 percent, and 91 percent). Using State Ease 360 software, the BBD of RSM was utilized to determine the best possible combination of input variables (voltage, speed of travel, and the proportion of CO_2 in the gas mixture) for the experimental work. As a function of the input parameters, correlations between the response parameters were created. Fit statistics were used to assess the forecasting correlation's performance, and an analysis of ANOVA was performed to confirm the importance of the created correlations. To verify the established relationships, an outside studentized plot was examined.

The State Ease 360 software's validation results for optimized input parameters were contrasted with the experimental results for the optimized parameter. The paper's outline is as follows: section 2 presents the experimental setup, methodology, and design of BBDs experiments. Section 3 depicts the results and discussion, which includes results of experimentation, development of correlation, ANOVA analysis, fit statistics, externally studentized residuals plot for the response parameters, outcomes of state ease 360 software, and experimentation for the optimized input parameters. Section 4 presents the conclusion of the present research work.

2. Experimental Setup, Methodology, and Design of Experiment

2.1. Experimental Setup

The 3-D model and experimental setup of the GMAW-based WAAM process are seen in Figure 1(a) and (b). The experiment's equipment included the working table, wire feeder, computer interface, automated nozzle controller, power supply, control unit, shielding gas cylinder, and welding torch. In the present investigation, shielding gas utilized for bead deposition comprised a mixture of varying percentages of Argon (99%. 95%, and 91%) and CO_2 (1%, 5%, and 9%). The software code was created and run through a computer interface for precise bead deposition.

The developed programme code controls the automated nozzle controller's travel along the X, Y, and Z coordinates through a computer interface. Before each programme run began, gas protection was introduced into the setup to prevent the build-up material from coming into contact with air gases. The versatile welding torch, which can move in a specific direction based on experimental requirements, was used to deposit beads on the base metal clamped to the work table from all sides. Metalloy 80B2 (chrome-moly steels), a gas-shielded metal-cored wire, was used in this study for bead deposition in one or more passes. The superior penetration and deposition rate of metal-cored wire over solid and flux-coated wire led to its selection. The chemical compound of metal-cored wire (Metalloy 80B2) is shown in Table 1. Hobart Brothers provided a 1.2 mm diameter Metalloy 80B2 wire (TRI-MARK).

2.2. Response Surface Methodology

Optimizing a process or system's operational parameters or designing an experiment properly are necessary for achieving the best possible performance. This minimizes the amount of time, money, and experimental iterations required to get the best possible performance. The optimization technique is a potent tool for determining the experiment's ideal operating conditions and parameters. The methodology or optimization technique used to design the tests or determine the ideal set of parameters must be economical.

[23] An effective and practical statistical tool, RSM assists the researcher in methodically creating a series of tests for operational parameter optimization. [24] The response variable is modelled by RSM as a function of several independent variables using the factorial approach and ANOVA. The ideal factorial variable setting to obtain the intended maximum or minimum response is determined using RSM. Using RSM to optimize parameters has several advantages, like being economically efficient, requiring fewer experiments, identifying the ideal circumstances, figuring out how the variables interact, making fitting easier, furnishing a visual representation, and more. BBDs are one of the RSM types utilized for optimization in this study.

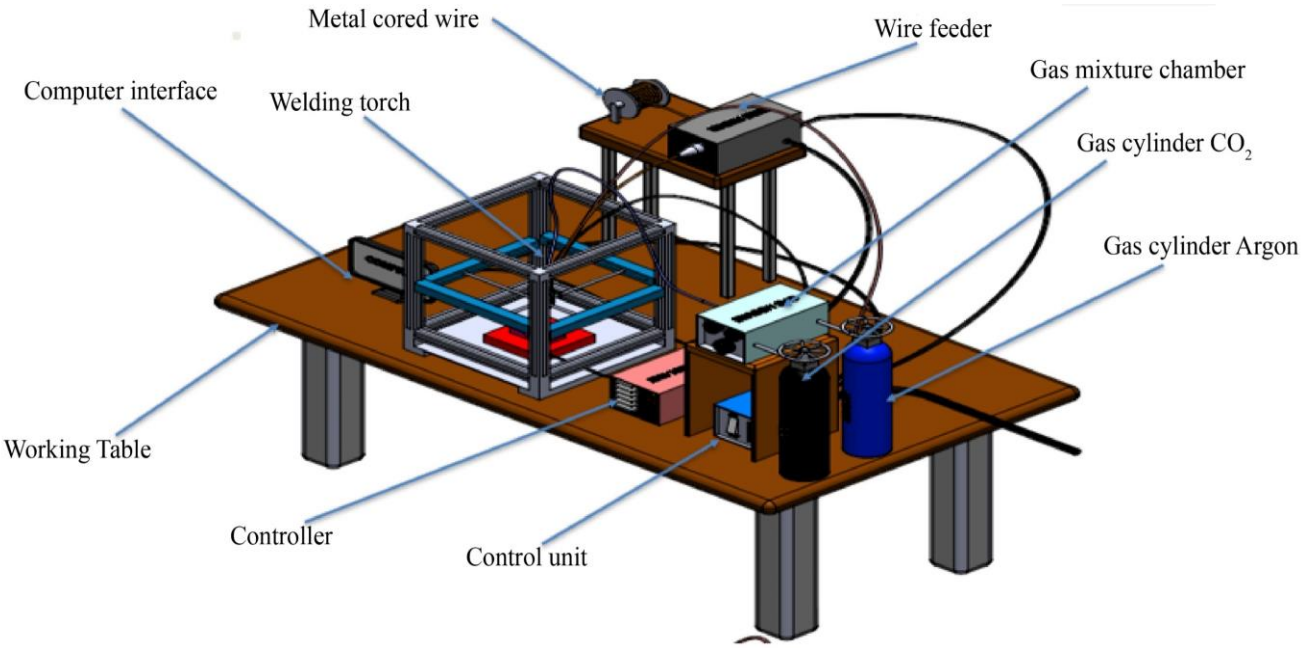

(a)

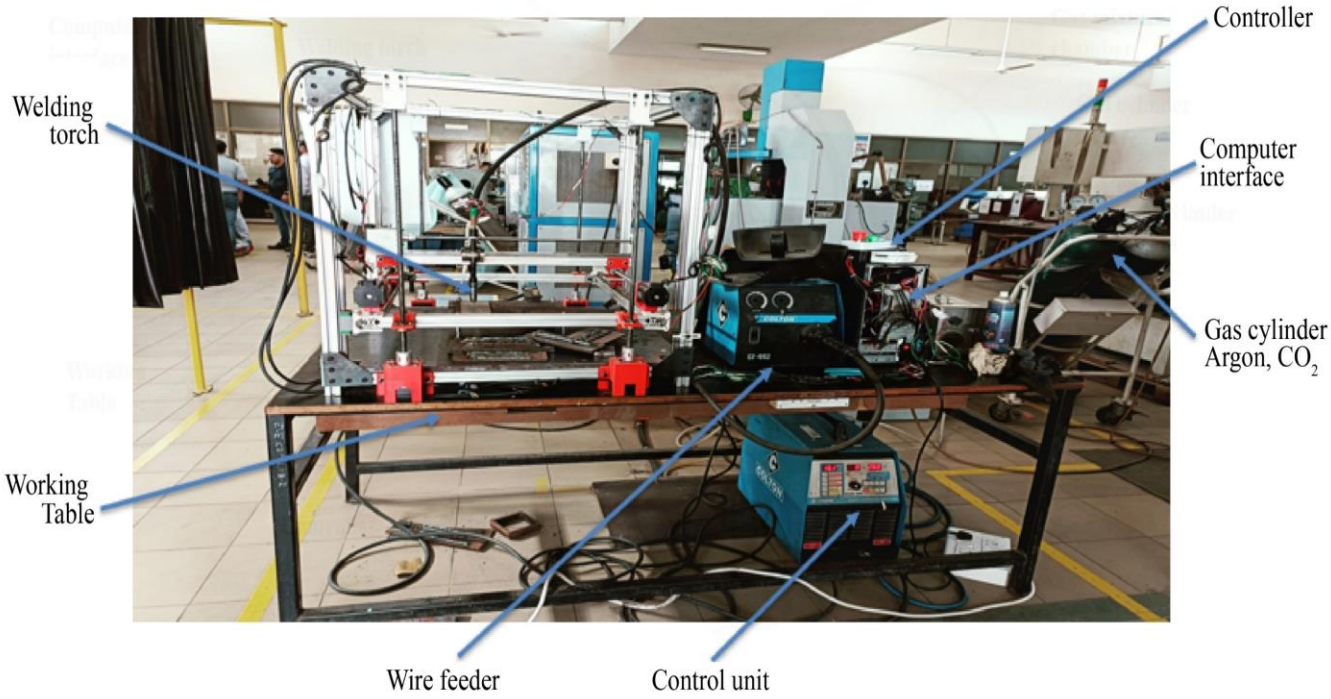

(b)

Fig. 1(a) 3-D model, (b) experimental setup of GMAW-based WAAM process.

Table 1. The chemical compound of Metalloy 80B2

Grade	Cr	Mn	Mo	C	Si	Fe
1.00 - 1.50% Chromium, 0.50% Molybdenum (Metal - cored wire)	1.36	0.82	0.5	0.06	0.29	Balance

2.3. Design of Experiment using Box-Behnken Designs

Higher-order response surfaces can be produced with fewer runs by fitting a quadratic model using the independent quadratic designs known as BBDs, which are experimental designs for RSM. Based on three-level incomplete factorial designs that need at least three components, the BBDs are a type of rotatable or nearly rotatable second-order designs. Treatment combinations are located in the centre of BBDs and at the halfway points of the process' edges. While the Depth Of Penetration (DOP), BH, and BW are selected as response parameters to examine the impact of process parameters, the voltage (V), travel speed (S), and percentage of CO_2 in gas mixture ratio are selected as input parameters for optimization. It was decided to vary the study's input parameters as follows: the percentage of CO_2 in the gas mixture ratio should be between 1 and 9 percent with a step size of 4 percent, the travel speed should be between 6 and 10 mm/s with a step size of 2 mm/s, and the voltage (V) should be between 22 and 26 V with a step size of 2 V. Other parameters, including arc length, bead length, and gas flow rate, were determined to be 3 mm, 150 mm each, and 15 L/min based on the system's machining capability and a literature review. An illustration of using BBD to examine how input variables affect response parameters can be found in Figure 2. For the optimization procedure, State Ease 360 software was utilized. The best system or process performance would be attained after 15 experimental runs, according to the BBDs. Table 2 shows the input variable combination for each run or best results.

..

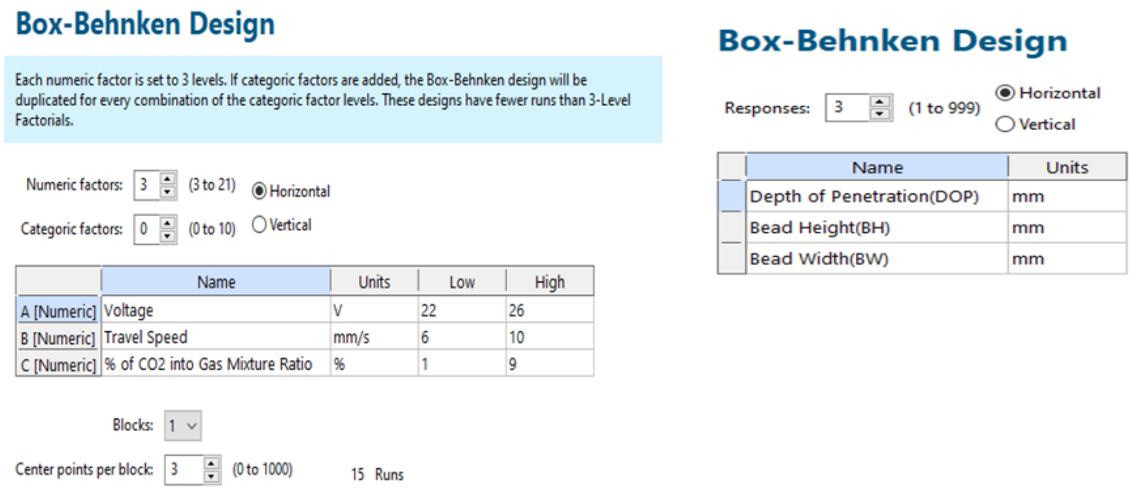

Fig. 2 Design of experiment using BBD

Table 2. Value of input parameter for various run

Run order	Standard order	Input parameter or Factor -1	Input parameter or Factor -2	Input parameter or Factor -3
		Voltage (V)	Travel Speed (mm/s)	% of CO_2 in the gas mixture ratio
1	15	24	8	5
2	11	24	6	9
3	2	26	6	5
4	13	24	8	5
5	8	26	8	9
6	7	22	8	9
7	12	24	10	9
8	10	24	10	1
9	1	22	6	5
10	9	24	6	1
11	6	26	8	1
12	5	22	8	1
13	14	24	8	5
14	4	26	10	5
15	3	22	10	5

3. Result and Discussion

3.1. Result of Experimentation

The experimental setup outlined in subsection 2.1 was used for 15 experimental runs, with the input parameter combinations anticipated using the BBDs technique (subsection 2.3) for optimal performance. For the 15 experimental runs, Figure 3 depicts the single-layered deposition of metal-cored wire Metalloy 80B2 on the base plate. Slices or cross-sections of single-layer deposition were used to quantify response variables such as DOP, BH, and BW. DOP, BH, and BW were among the response characteristics measured using the optical microscopy technique. Table 3 shows the average of the three measured response parameter values for each experimental run. Each response parameter was assessed three times to prevent measurement error. The experiment's measured value was within a range of ± 5 percent.

3.2. Correlation for DOP, BH, and BW

The response surface model, which is shown in Equation (1), Equation (2), and Equation (3)**,** was created using RSM to determine the connection between the input parameters (voltage, travel speed, and the percentage of CO_2 in the gas mixture) and response parameters (DOP, BH, and BW). The DOP correlation shows a nonlinear relationship between the input and response parameters by including the input variable's linear, mixed, and quadratic terms. On the other hand, BH and BW's correlation shows a linear relationship with the input variables. For the researcher working on the study article, the established correlations aid in predicting the response parameter before doing the experiment, which may be used to maximize process performance. This will save time, money, and time for the researchers' resources (financial, physical, and infrastructure, etc.) and industrial adaptations.

Equation (1)

$$DOP = +7.61595 - 0.588794 * A - 0.150889 * B - 0.036556 * C + 0.000137 * A * B - 0.001981 * A * C + 0.009078 * B * C + 0.014520 * A^2 + 0.004451 * B^2 + 0.002928 * C^2$$

Equation (2)

$$BH = -2.69810 + 0.094375 * A + 0.821250 * B + 0.049687 * C$$

Equation (3)

$$BW = +28.0809 - 0.935000 * A + 0.399375 * B + 0.110938 * C$$

Where A, B, and C indicate voltage (V), travel speed (mm/s), and % of CO_2 in the gas mixture (%).

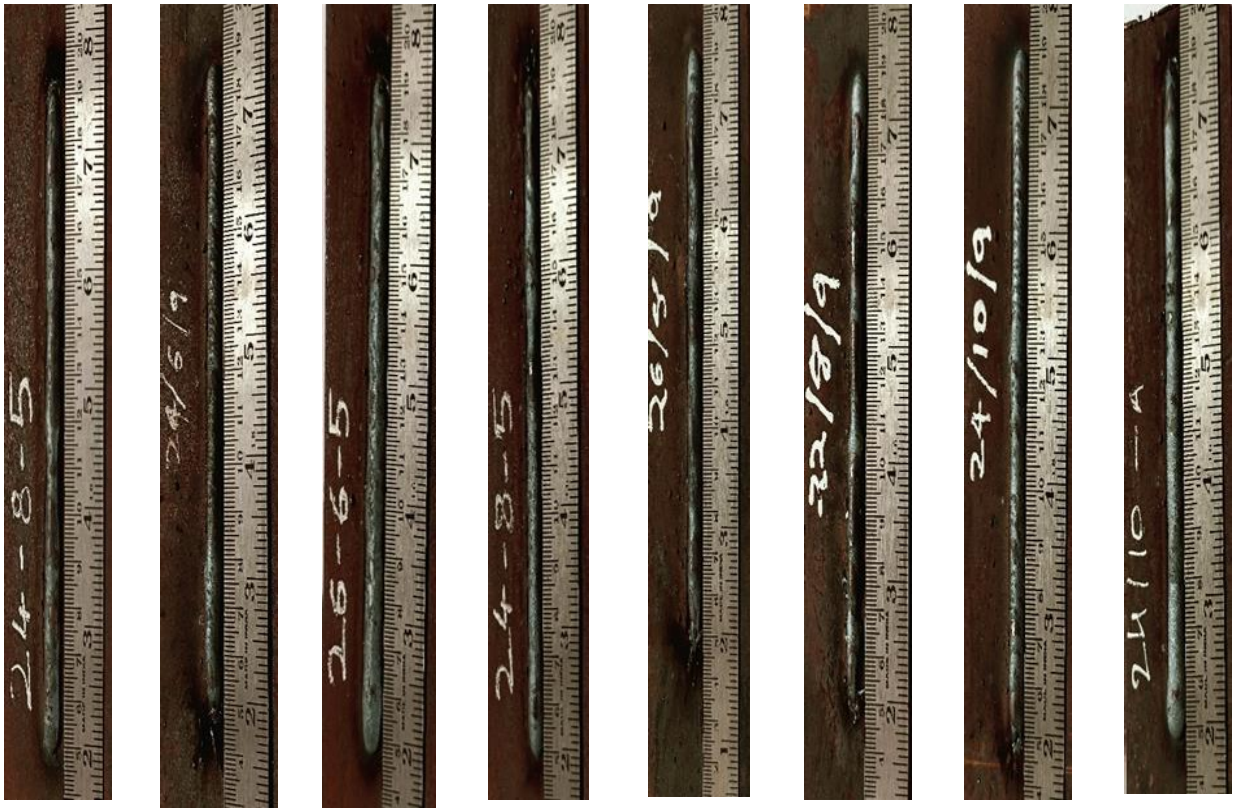

Run order-1 Run order-2 Run order-3 Run order-4 Run order-5 Run order-6 Run order-7 Run order-8

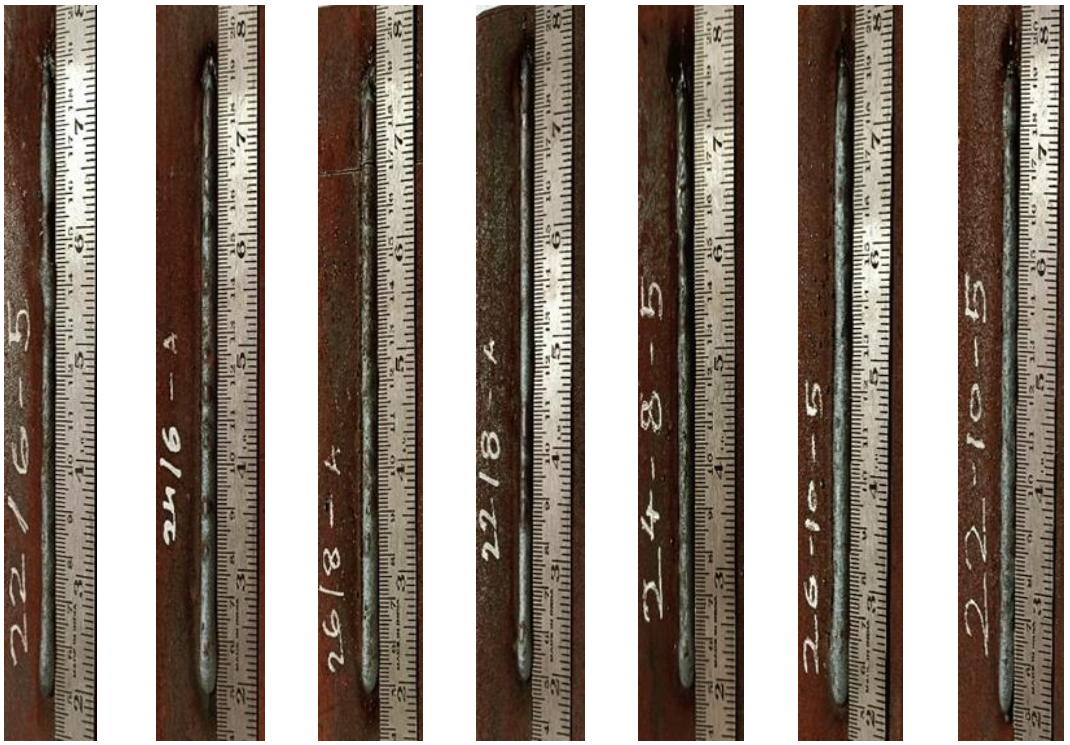

Run order-9 Run order-10 Run order-11 Run order-12 Run order-13 Run order-14 Run order-15

Fig. 3 Single-layered deposition of metal-cored wire Metalloy 80B2 on the base plate

Table 3. Output of experimentations

Run order	Standard order	Input-1	Input-2	Input-3	Output-1	Output-2	Output-3
		Voltage (V)	Travel Speed (mm/s)	% of CO_2 into the gas mixture	DOP (mm)	BH (mm)	BW (mm)
1	15	24	8	5	0.9603	6.27	9.61
2	11	24	6	9	1.1034	4.95	8.49
3	2	26	6	5	1.3198	4.93	6.97
4	13	24	8	5	0.9777	6.61	9.26
5	8	26	8	9	1.3326	6.72	8.21
6	7	22	8	9	0.9625	6.72	12.41
7	12	24	10	9	1.1294	7.81	10.67
8	10	24	10	1	0.8172	8.55	10.02
9	1	22	6	5	0.8971	4.95	10.14
10	9	24	6	1	1.0817	4.11	8.11
11	6	26	8	1	1.2156	6.72	7.36
12	5	22	8	1	0.7760	5.23	10.74
13	14	24	8	5	0.9668	6.49	9.46
14	4	26	10	5	1.1923	7.88	7.6
15	3	22	10	5	0.7674	7.84	11.81

Table 4. ANOVA results for DOP

Source	Sum of squares	Degree of freedom	Mean square	F-value	p-value	
Model	0.4288	9	0.0476	85.22	< 0.0001	Significant
A - Voltage	0.3159	1	0.3159	564.99	< 0.0001	
B - Travel speed	0.0307	1	0.0307	54.94	0.0007	
C - % of CO_2 into gas mixture	0.0406	1	0.0406	72.57	0.0004	
AB	1.210E-06	1	1.210E-06	0.0022	0.9647	
AC	0.0010	1	0.0010	1.80	0.2377	
BC	0.0211	1	0.0211	37.74	0.0017	
A^2	0.0125	1	0.0125	22.28	0.0052	
B^2	0.0012	1	0.0012	2.09	0.2076	
C^2	0.0081	1	0.0081	14.50	0.0125	
Residual	0.0028	5	0.0006			
Lack of fit	0.0026	3	0.0009	11.39	0.0818	Not significant
Pure error	**0.0002**	**2**	**0.0001**			
Corrected Total	**0.4316**	**14**				

Table 5. ANOVA results for BH

Source	Sum of squares	Degree of freedom	Mean square	F-value	p-value	
Model	22.18	3	7.39	39.81	< 0.0001	Significant
A – Voltage	0.2850	1	0.2850	1.53	0.2412	
B - Travel speed	21.58	1	21.58	116.20	< 0.0001	
C - % of CO_2 into gas mixture	0.3160	1	0.3160	1.70	0.2187	
Residual	2.04	11	0.1857			
Lack of fit	1.98	9	0.2204	7.41	0.1245	Not significant
Pure error	0.0595	2	0.0297			
Corrected total	24.23	14				

Table 6. ANOVA results for BW

Source	Sum of squares	Degree of freedom	Mean square	F-value	p-value	
Model	34.65	3	11.55	69.25	< 0.0001	Significant
A - Voltage	27.98	1	27.98	167.70	< 0.0001	
B - Travel speed	5.10	1	5.10	30.60	0.0002	
C - % of CO_2 into gas mixture	1.58	1	1.58	9.44	0.0106	
Residual	1.83	11	0.1668			
Lack of fit	1.77	9	0.1970	6.39	0.1426	Not significant
Pure error	0.0617	2	0.0308			
Corrected total	36.49	14				

3.3. ANOVA for DOP, BH, and BW

In subsection 3.1, the F-value and p-value for the established correlation are predicted using the ANOVA. The ANOVA analysis is seen in Table 4 for DOP, Table 5 for BH, and Table 6 for BW. The acceptance or rejection of the null hypothesis is indicated by the F-value. The high F-value indicates the model's importance. Assuming the null hypothesis is correct, the p-value calculates the likelihood of getting the observed outcomes. If the p-value for the model is less than 0.05, it is deemed statistically significant. The F-value and p-value for the DOP obtained from ANOVA are 85.22 and < 0.0001, indicating the model/correlation of DOP is significant. From the result of ANOVA for DOP, voltage (represented by parameter A) is found to be more important than the other input parameters in the model/correlation of DOP. The F-value and p-value for the BH obtained from ANOVA are 39.81 and < 0.0001, indicating the model/correlation of BH is significant. From the result of

ANOVA for BH, travel speed (represented by parameter B) is found to be more important than the other input parameters in the model/correlation of BH. The F-value and p-value for the BW obtained from ANOVA are 69.25 and < 0.0001, indicating the model/correlation of BW is significant. From the result of ANOVA for BW, voltage (represented by parameter A) is found to be more important than the other input parameters in the model/correlation of BW.

The lack of fit indicates the variation of the designed point about predicated value. It should be insignificant for the model to fit well in experimental data, indicating the lower value of lack of fit is preferable. The F-value of lack of fit obtained from ANOVA for the DOP, BH, and BW was 11.39, 7.42, and 6.39; and the p-value of lack of fit obtained from ANOVA for the DOP, BH, and BW was 0.0818, 0.1245, and 0.1426, indicating not significant or predicated model/correlations are adequate.

3.4. Fit statistics for DOP, BH and BW

Table 7 depicts the fit statistics for the DOP, BH, and BW. Fit statistics indicate statistical values utilized to assess the effectiveness of the forecasting model by comparing actual data to the predictions. The predicted R2 represent how the regression model/correlation predicts/accurate response for new observations. The adjusted R2 accounts/penalizes the variables that are not significant in the regression model/correlation. In other words, adjusted R2 provides an accurate model/correlation that fits the current data, whereas predicted R2 determines how likely that model/correlation is accurate for future data.

The adjusted R2 and predicted R2 values for DOP were 0.9819 and 0.9013, indicating that the model/correlation is accurate for predicting response parameters as the difference between adjusted R2 and predicted R2 is less than 0.2. The adequate precision represents the signal-to-noise ratio. The adequate precision value for DOP was 28.196, higher than 4, indicating adequate model discrimination.

Table 7. Fit Statistics for DOP, BH and BW

Fit statistics	DOP	BH	BW
Standard Deviation	0.0236	0.4310	0.4084
Mean	1.03	6.39	9.39
Coefficient of variance (%)	2.29	6.75	4.35
Coefficient of determination (R2)	0.9935	0.9157	0.9497
Adjusted R^2	0.9819	0.8927	0.9360
Predicted R^2	0.9013	0.8225	0.8942
Adequate precision	28.1957	16.5467	25.3067

3.5. Externally Studentized Residuals Plot for DOP, BH, and BW

Studentized residuals are the ratio of residual (difference between the predicted value of the parameter to the actual value) to the estimation of its standard deviation. Studentized residuals are categorized as externally studentized residuals and internally studentized residuals. Internally, studentized residuals utilize the mean square error for model/correlation based on all observations, whereas externally, studentized residuals utilize the mean square error based on outlier observations deleted. Figure 4, Figure 12, and Figure 20 represent the normal probability graph vs. externally studentized residuals for DOP, BH, and BW. The plots show that the majority of residuals are well-behaved, nearer to straight lines or normally distributed, indicating that the model/correlation is valid. Figure 5, Figure 13, and Figure 21 represent the plot of externally studentized residuals vs. predicted for DOP, BH, and BW. The plots show that the majority of residuals are well-behaved and randomly dispersed around the zero line and within the horizontal band, indicating that the model/correlation is valid.

Figure 6, Figure 14, and Figure 22 represent the plot of externally studentized residuals vs. run numbers for DOP, BH, and BW. The plots show that the majority of residuals are well-behaved, randomly dispersed/patterned around the zero line and within the horizontal band, indicating that the model/correlation is valid. Figure 7, Figure 15, and Figure 23 represent the plot of externally studentized residuals vs. input parameters - voltage, travel speed, and % of CO_2 into the gas mixture for DOP. Figure 15, Figure 16, and Figure 17 represent the plot of externally studentized residuals vs. input parameters - voltage, travel speed, % of CO_2 into the gas mixture for BH. Figure 23, Figure 24, and Figure 25 represent the plot of externally studentized residuals vs. input parameters - voltage, travel speed, % of CO_2 into the gas mixture for BW. The plots show that the majority of residuals are well-behaved and within the horizontal band, indicating that the model/correlation is valid. Figure 10, Figure 18, and Figure 26 represent the box-cox plots for DOP, BH, and BW, respectively. The Box-Cox transformation is a statistical technique used to increase the precision of model/correlation predictions by converting non-normal data into a normal distribution. In the Box-Cox plot, the vertical line corresponding to Lambda = 1 indicates that it is equivalent to the original data. If a 95% confidence interval for the optimal Lambda includes a vertical line corresponding to Lambda = 1, it indicates no transformation is necessary; otherwise, transformation is appropriate. The plots show that the vertical line corresponding to Lambda = 1 within the 95% confidence interval, indicating no transformation is necessary. Figure 11, Figure 19 and Figure 27 represents the plot of externally studentized residuals predicted vs. actual for DOP, BH, and BW. The externally studentized residuals predicted vs. actual utilized to visualize the performance of the model/correlation; if predictions are perfect, then the point

lies near a straight line with a slope of 1. The plots show that residuals are closer to a straight line with a slope of 1, indicating that the predicted value using model/correlation is closer to the actual value, implying that model/correlation is valid.

3.6. Outcomes of Stat-Ease Software 360 and Experimentation for Optimized Input Parameters

The higher the value of DOP, the higher the value of BH, and the lesser the value of BH, the more desirable the optimum outcomes. Figure 28 represents the contour plot of desirability, DOP, BH, and BW for voltage vs. travel speed. Desirability was observed higher for the high value of voltage and travel speed. The high value of DOP was observed for a high voltage value, which increases with an increase in travel speed, achieves maximum for optimum value, and then decreases. The high value of BH was observed for the high value of travel speed, which decreased with an increase in voltage. The lower value of BW was observed for the high value of voltage and low value of travel speed. Figure 29 represents the contour plot of desirability, DOP, BH, and BW for voltage vs. % of CO_2 in the gas mixture. Desirability was observed to be higher for the high voltage and % of CO_2 in the gas mixture. The high value of DOP was observed for a high value of voltage and % of CO_2 in the gas mixture. A high value of BH was observed for the high voltage and % of CO_2 in the gas mixture. The lower value of BW was observed for the high value of voltage and low value of % of CO_2 in the gas mixture. Figure 30 represents the contour plot of desirability, DOP, BH, and BW for travel speed vs. % of CO_2 in the gas mixture. Desirability was observed higher for the high value of travel speed and % of CO_2 in the gas mixture. The high value of DOP was observed for a low value of travel speed and a high value of % of CO_2 in the gas mixture. The high value of BH was observed for the high value of travel speed and % of CO_2 in the gas mixture. The lower value of BW was observed for the high value of travel speed and % of CO_2 in the gas mixture.

Table 8 depicts the outcomes for the optimized value of input parameters using Stat Ease 360 software. Stat-Ease 360 software determined a total of 51 solutions, out of those optimum outcomes of DOP = 1.320 mm, BH = 8.381 mm, BW = 8.687 mm for the input parameter of voltage = 26 V, travel speed = 10 mm/s, % of CO_2 into gas mixture = 8.317% was chosen with the desirability of 0.895 by software as optimized output. Figure 31 represents the ramps graph for the optimum input parameters and optimum outcomes obtained from the State Ease 360 software. For the optimum input parameters (voltage = 26 V, travel speed = 10 mm, and % of CO_2 into gas mixture = 8.317) obtained from the State Ease 360 software, the experimental work for the optimum input parameter of voltage = 26 V, travel speed = 10 mm, and % of CO_2 into gas mixture = 8 (due to limitation in setting in an experiment setup) was conducted in five sets. The outcomes of the experimental set are presented in Table 9. The best result of experimentation was found within the range of ± 5% of results obtained from the State Ease 360 software. The multilayer structure (length and width) obtained from experimentation is presented in Figure 32, and the structure was found free from disbanding.

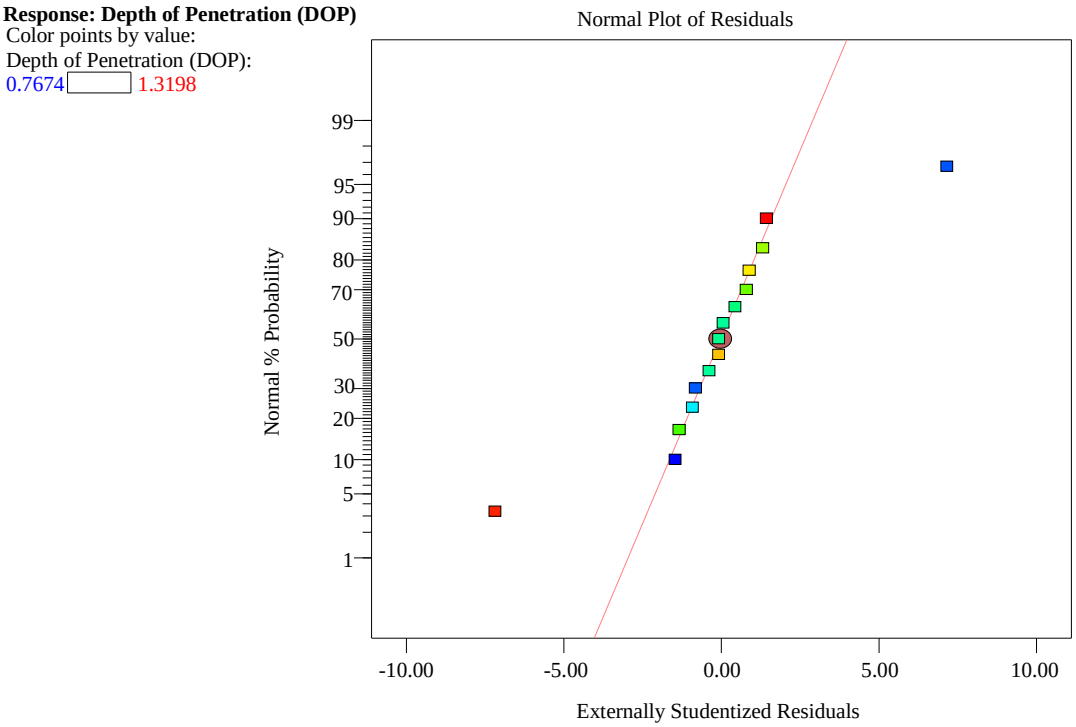

Fig. 4 Plot of normal probability vs. Externally studentized residuals for DOP

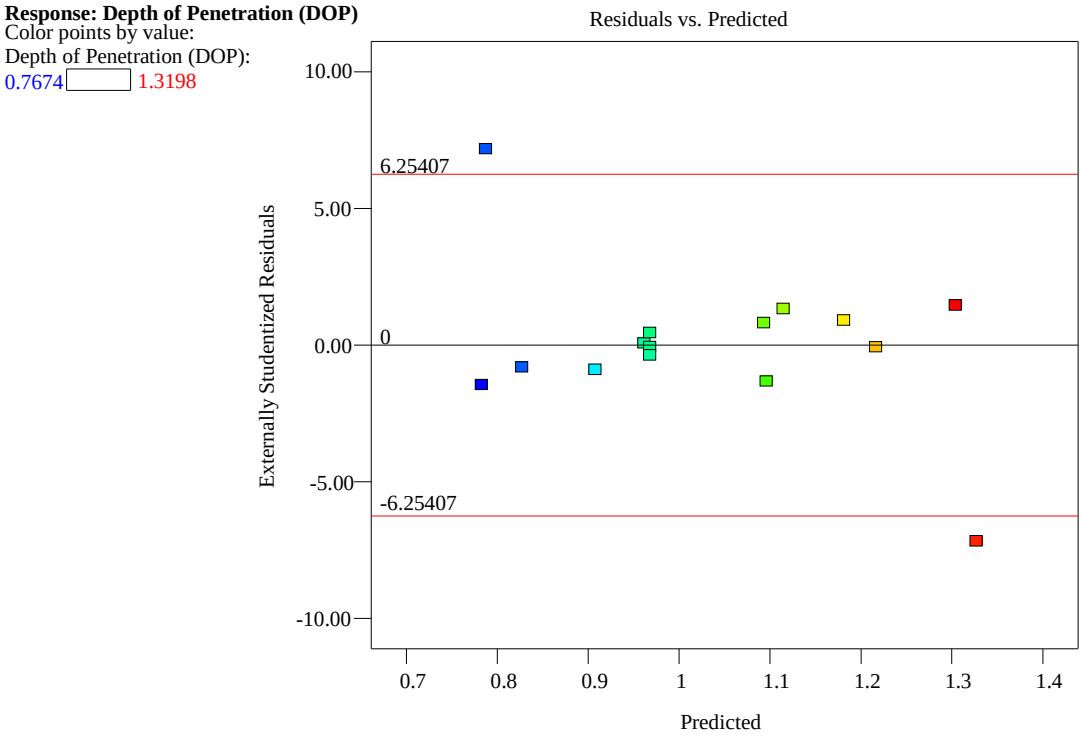

Fig. 5 Plot of externally studentized residuals vs. Predicted for DOP

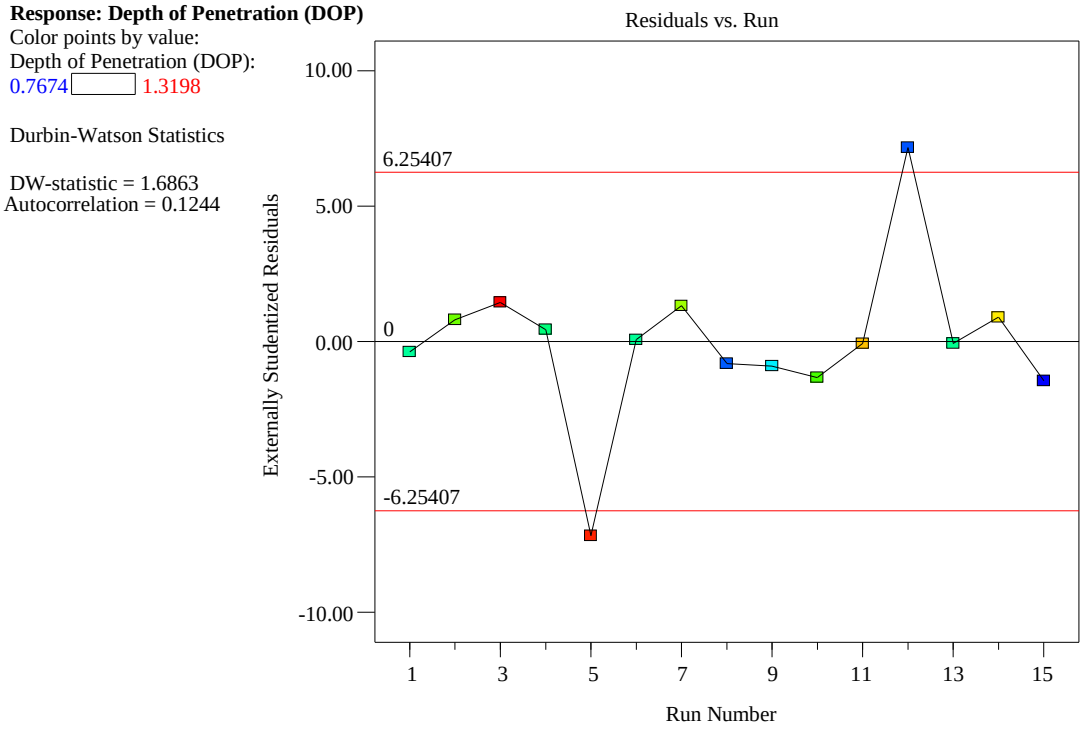

Fig. 6 Plot of externally studentized residuals vs. Run number for DOP

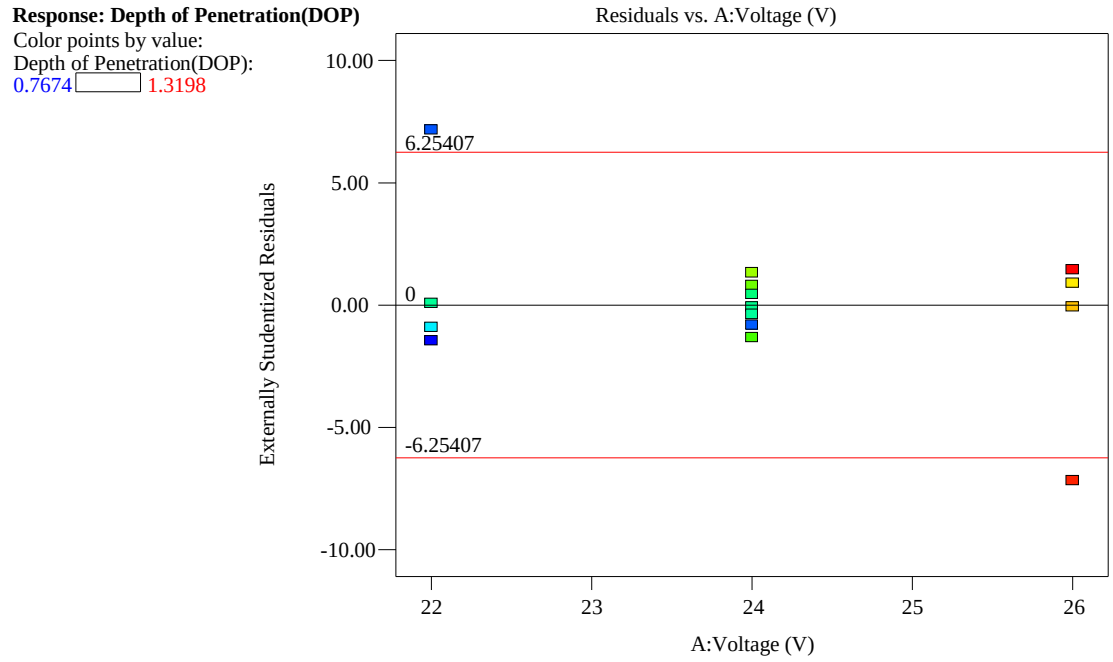

Fig. 7 Plot of externally studentized residuals vs. Input variable – voltage for DOP

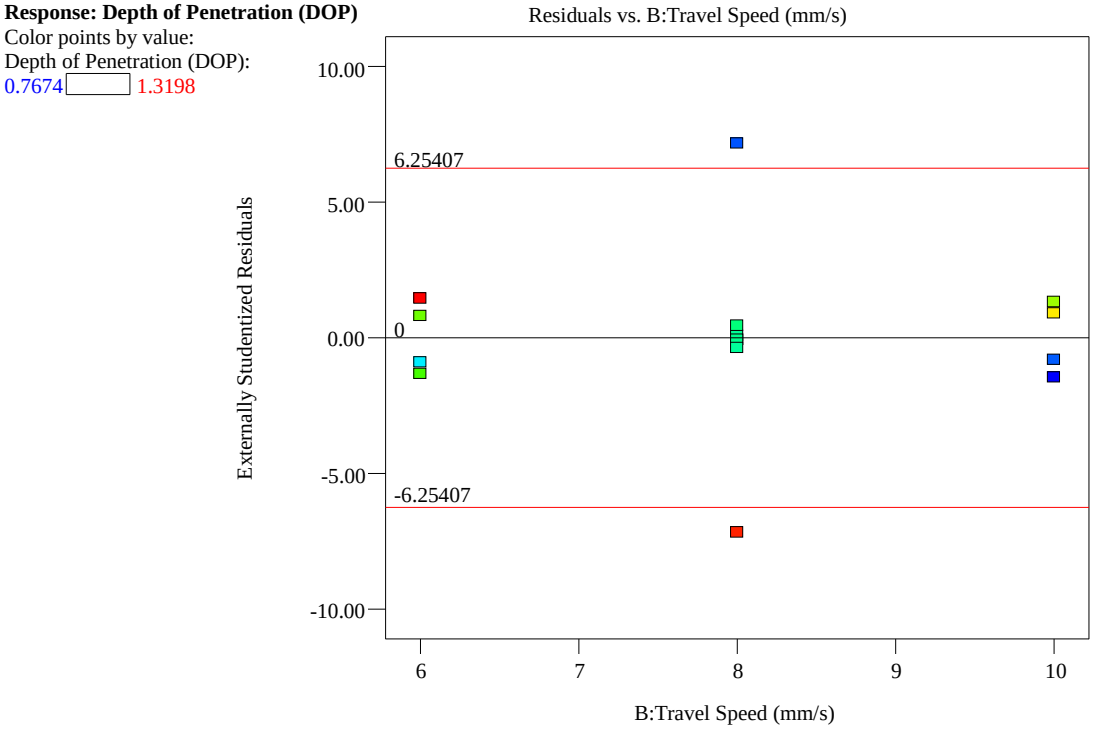

Fig. 8 Plot of externally studentized residuals vs. Input variable – travel speed for DOP

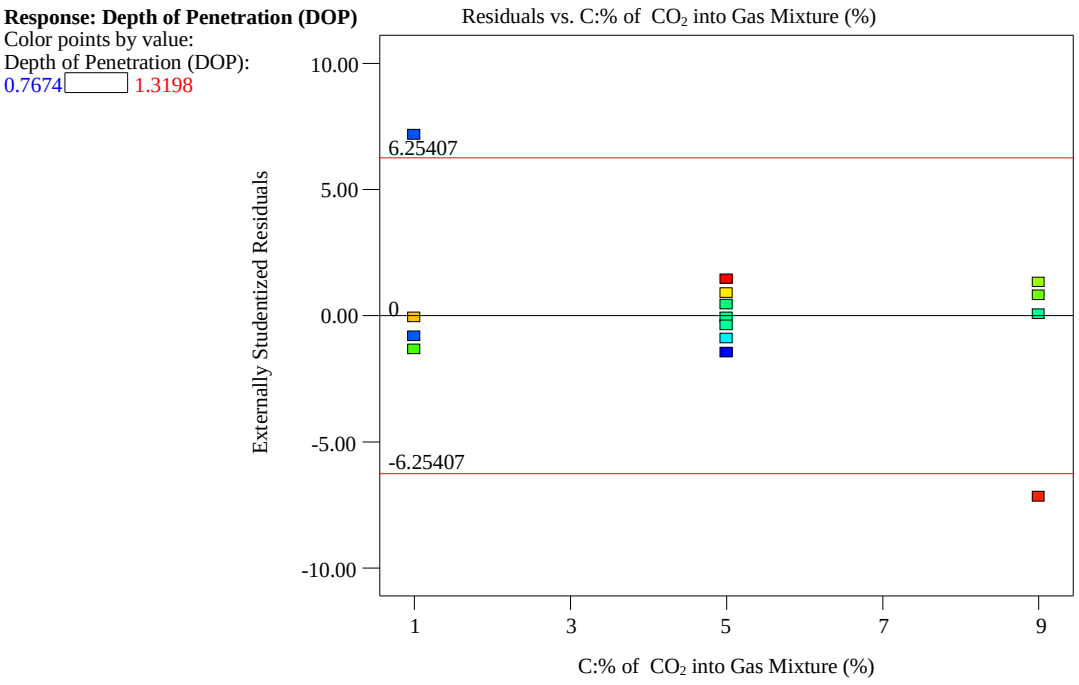

Fig. 9 Plot of externally studentized residuals vs. Input variable – % of CO_2 into the gas mixture for DOP

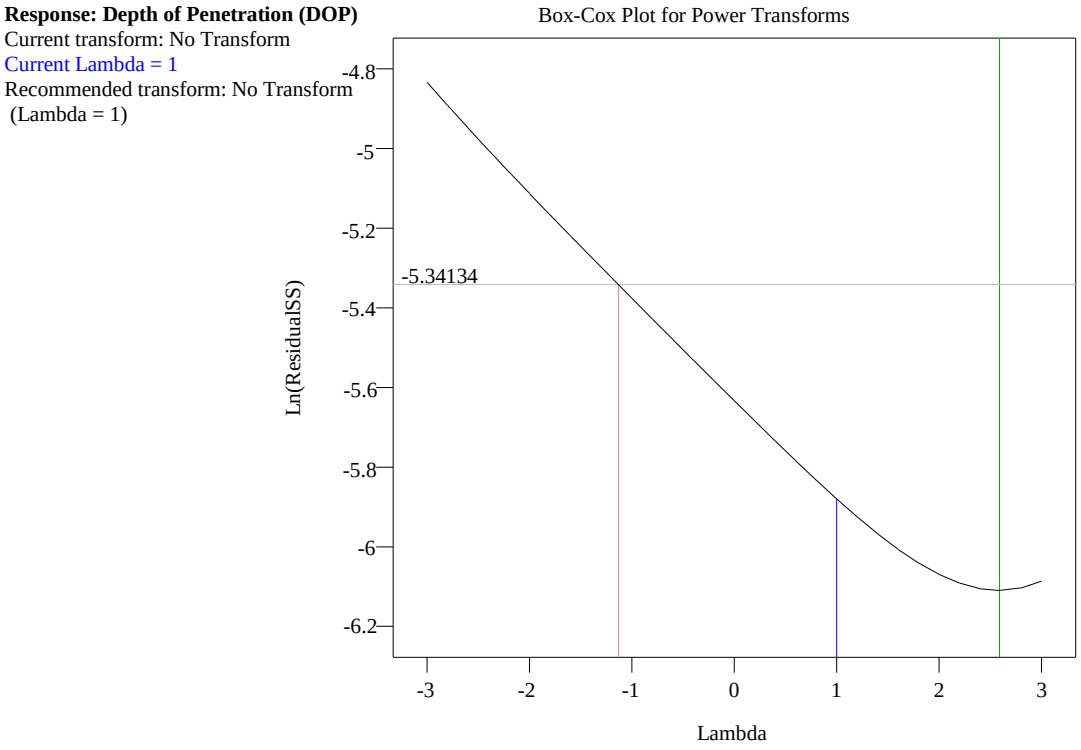

Fig. 10 Box-cox plot for DOP

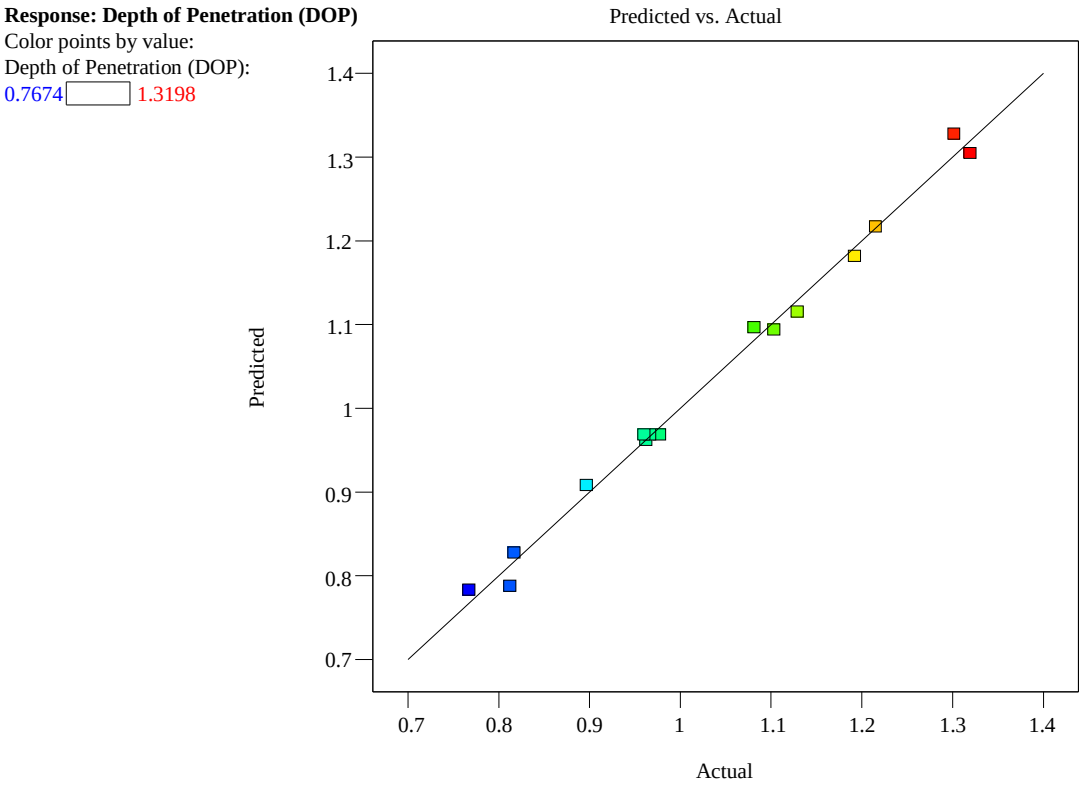

Fig. 11 Externally studentized residuals plot - predicted vs. Actual for DOP

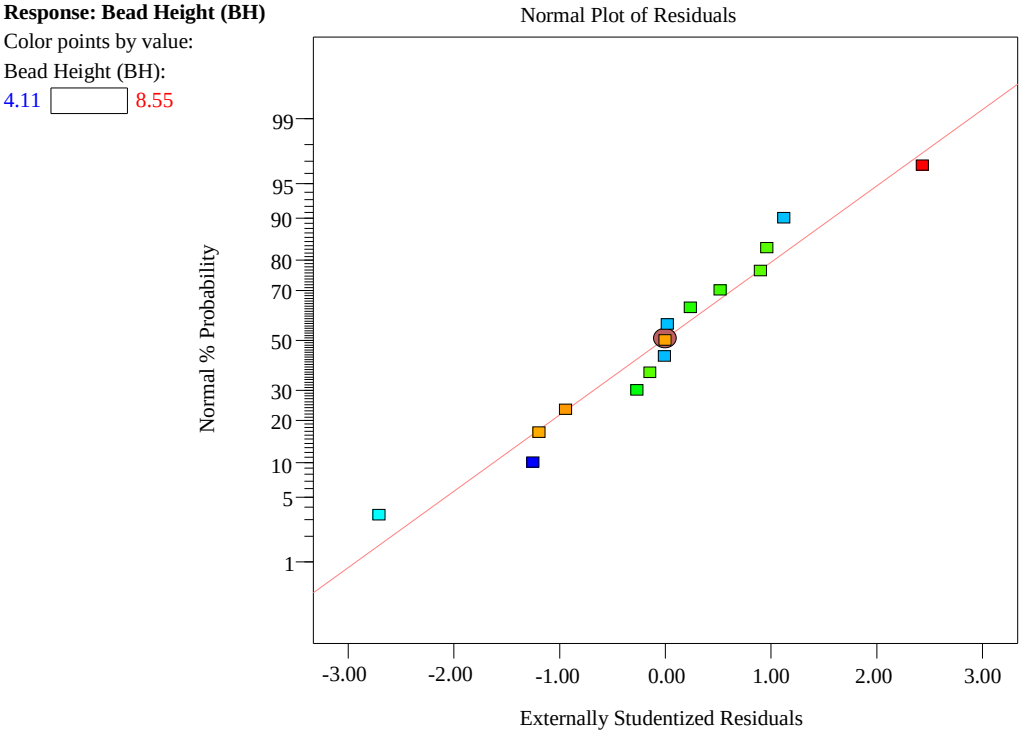

Fig. 12 Plot of normal probability vs. Externally studentized residuals for BH

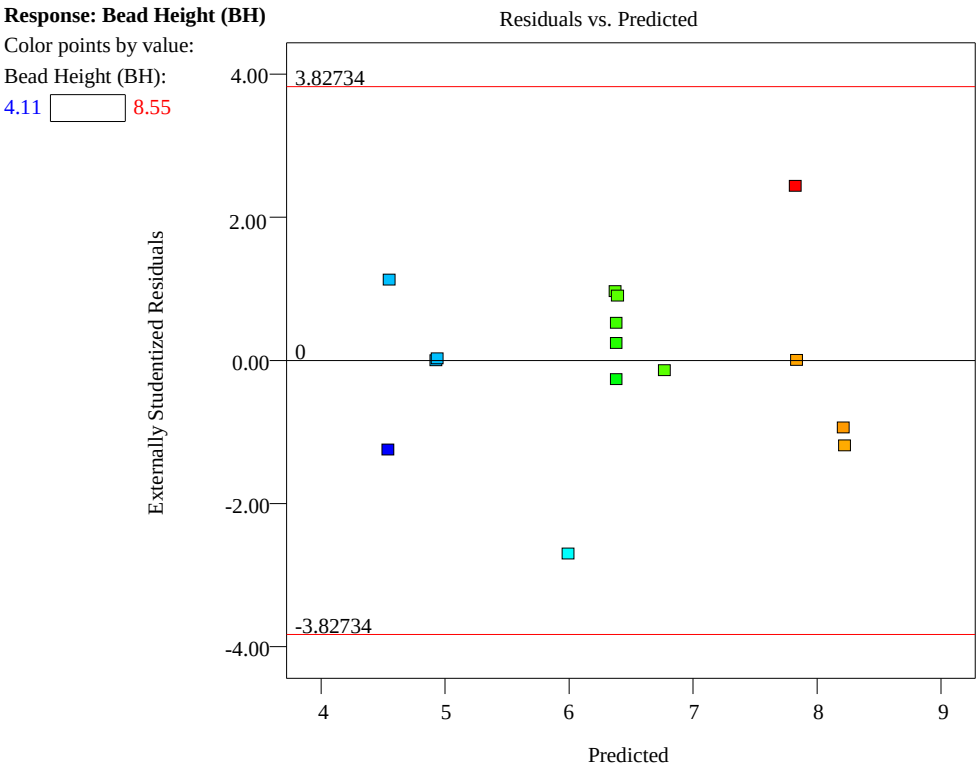

Fig. 13 Plot of externally studentized residuals vs. Predicted for BH

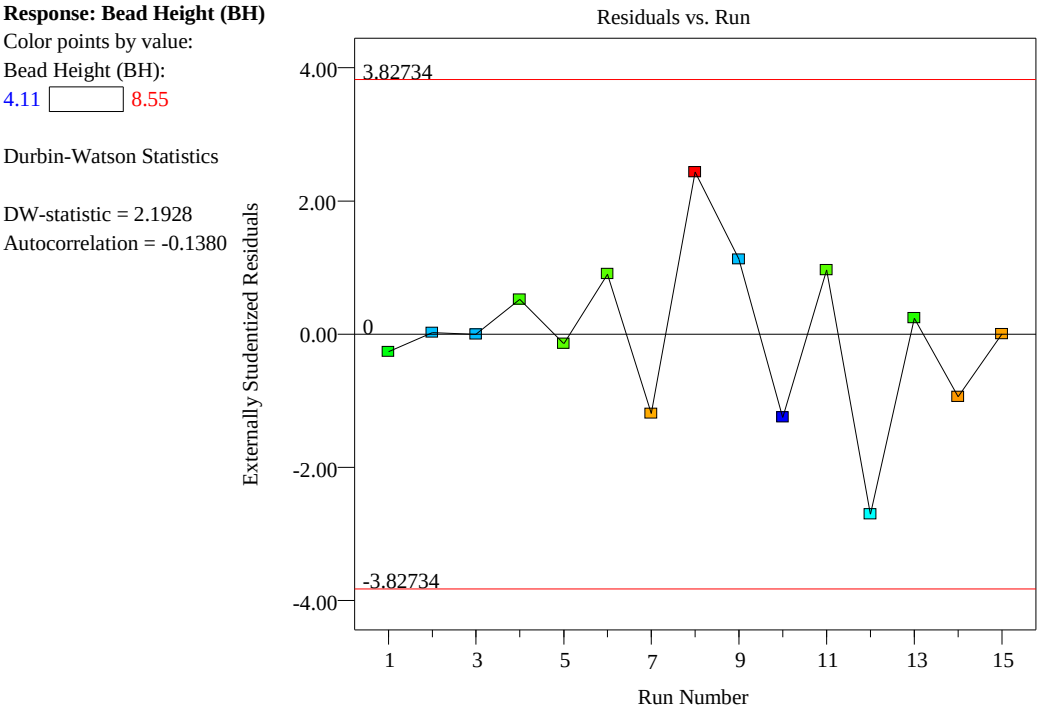

Fig. 14 Plot of externally studentized residuals vs. Run number for BH

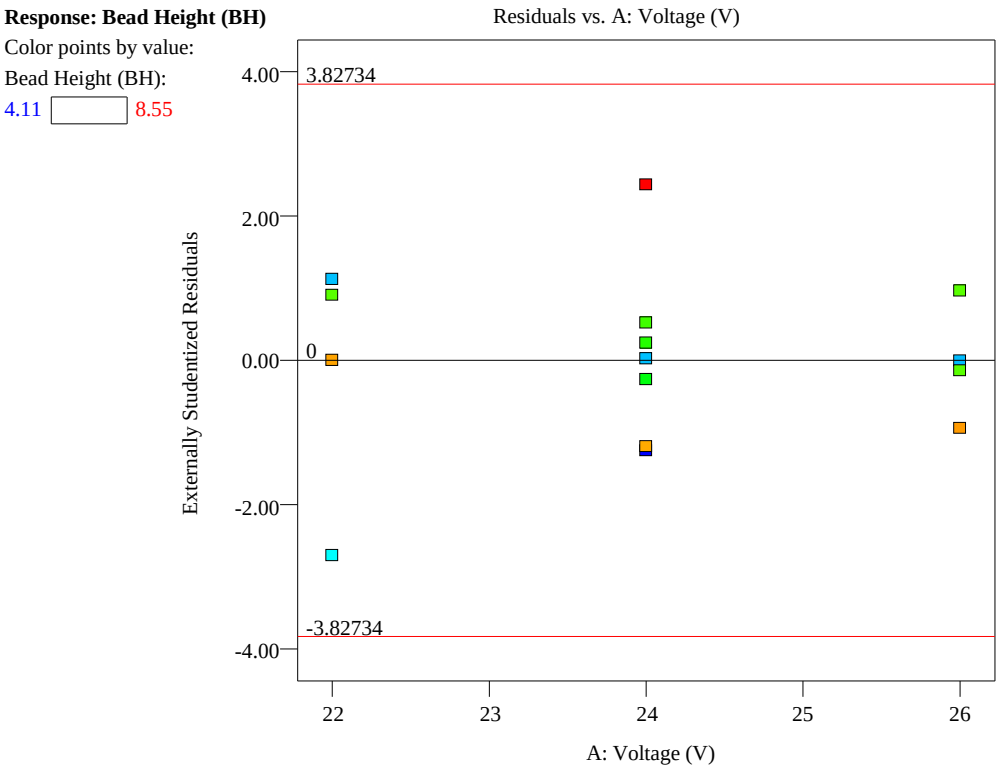

Fig. 15 Plot of externally studentized residuals vs. Input variable – voltage for BH

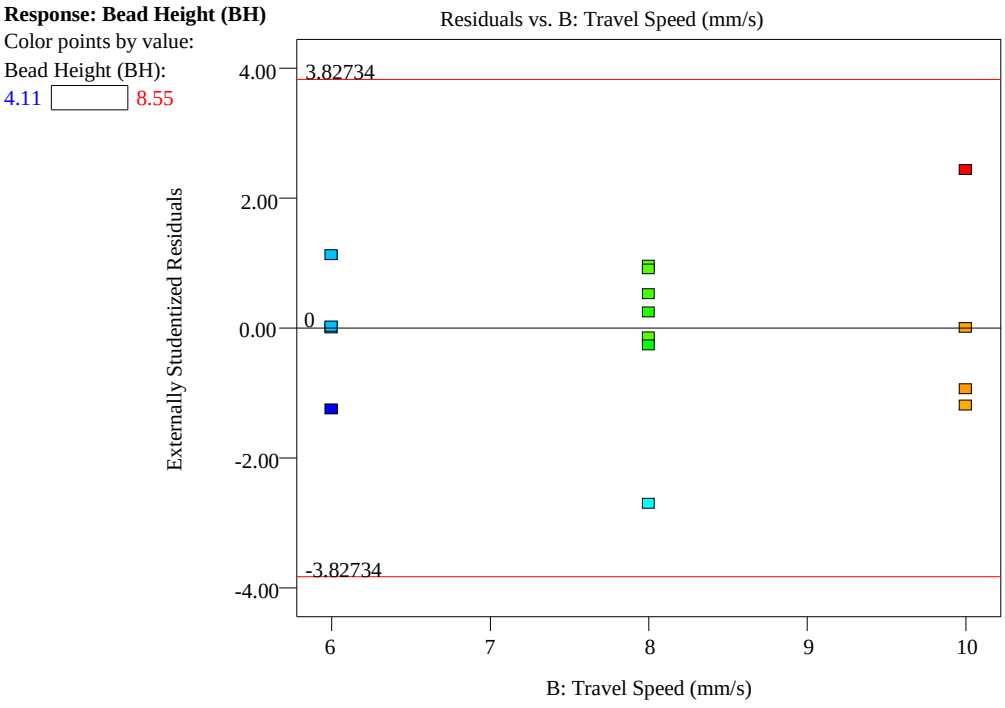

Fig. 16 Plot of externally studentized residuals vs. Input variable – travel speed for BH

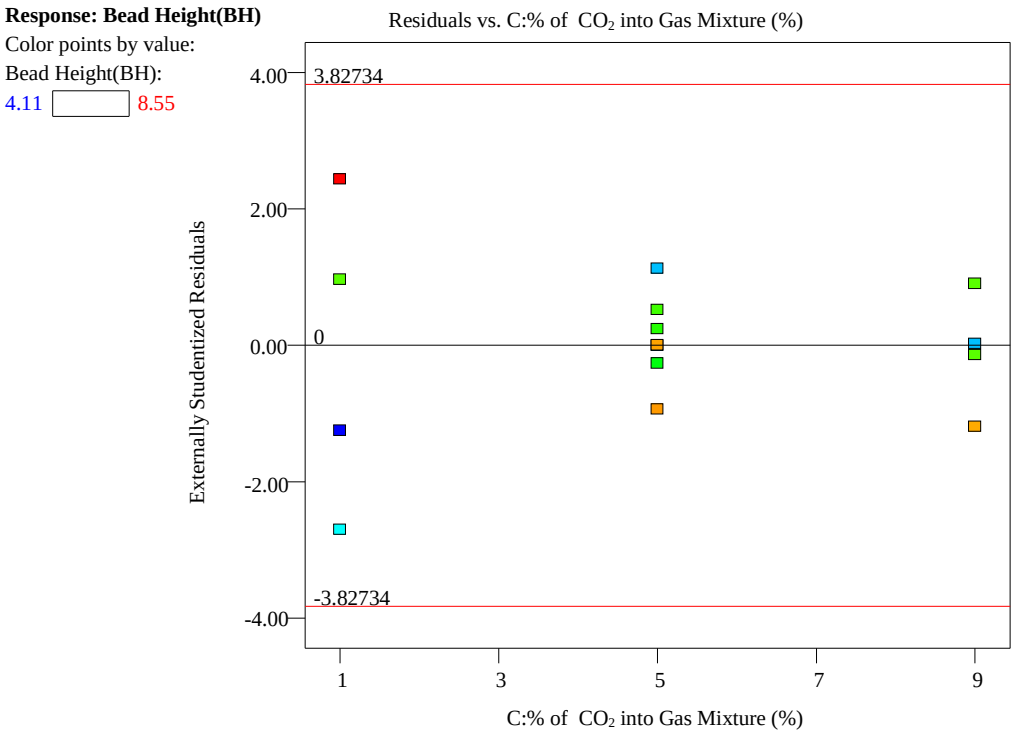

Fig. 17 Plot of externally studentized residuals vs. Input variable – % of CO_2 into the gas mixture for BH

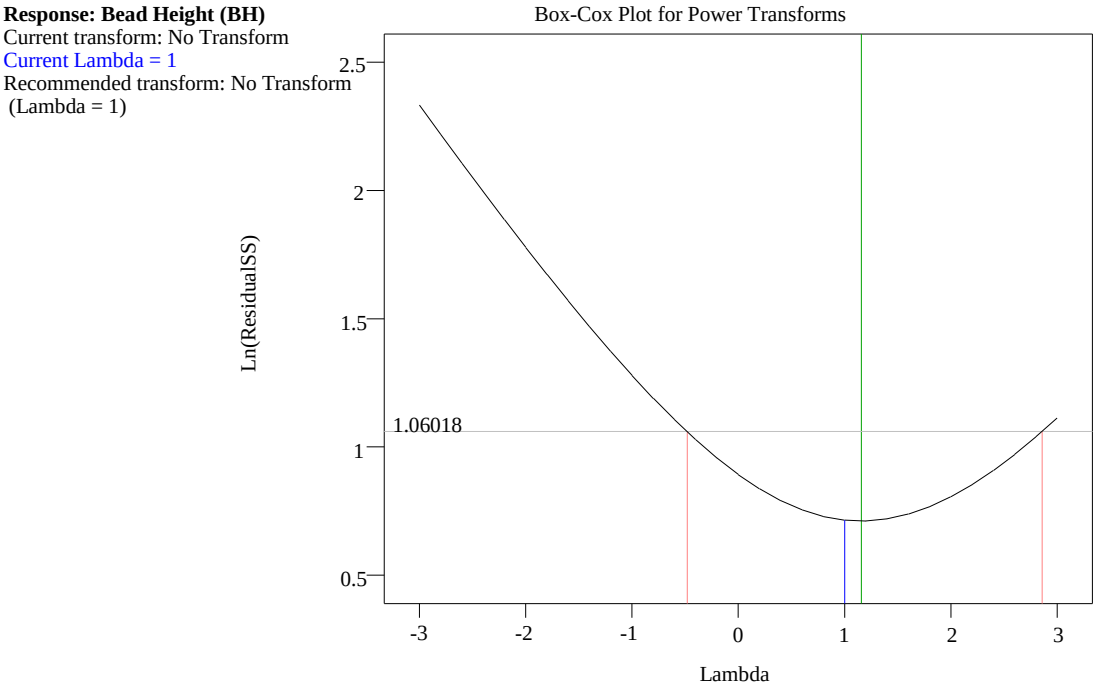

Fig. 18 Box-cox plot for BH

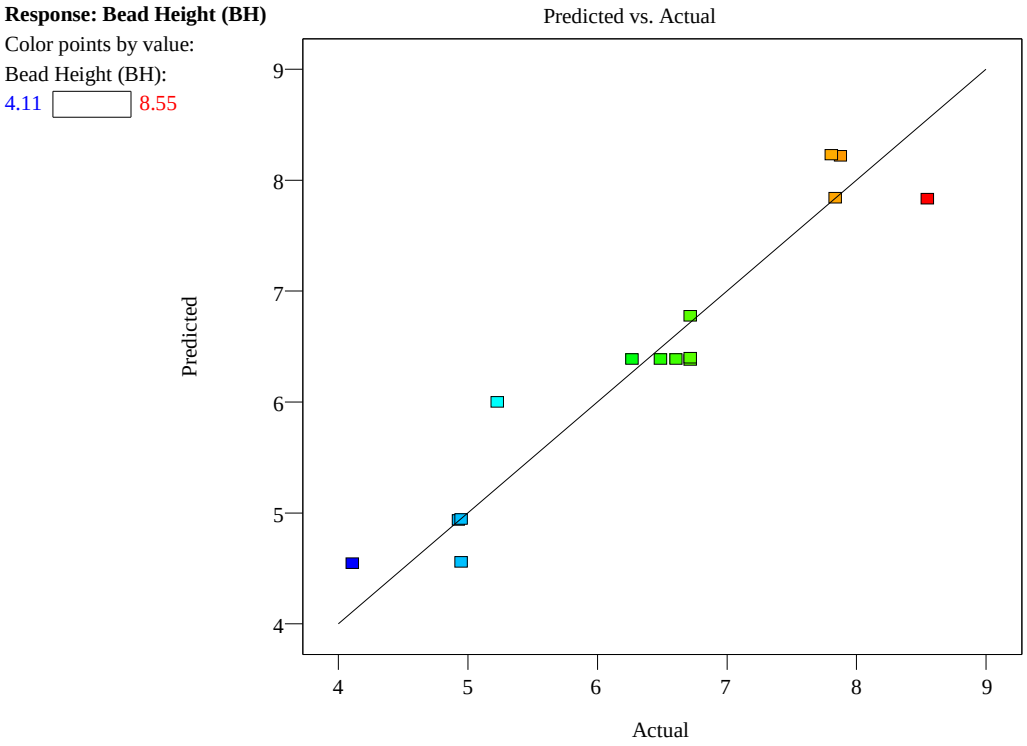

Fig. 19 Externally studentized residuals plot – predicted vs. Actual for BH

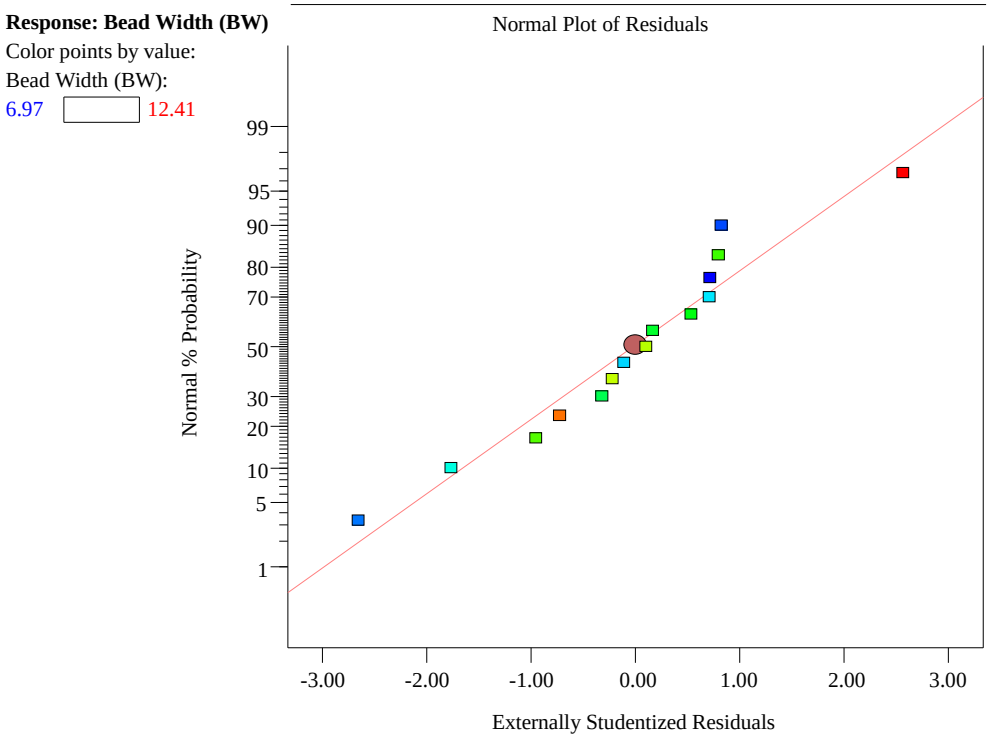

Fig. 20 Plot of normal probability vs. Externally studentized residuals for BW

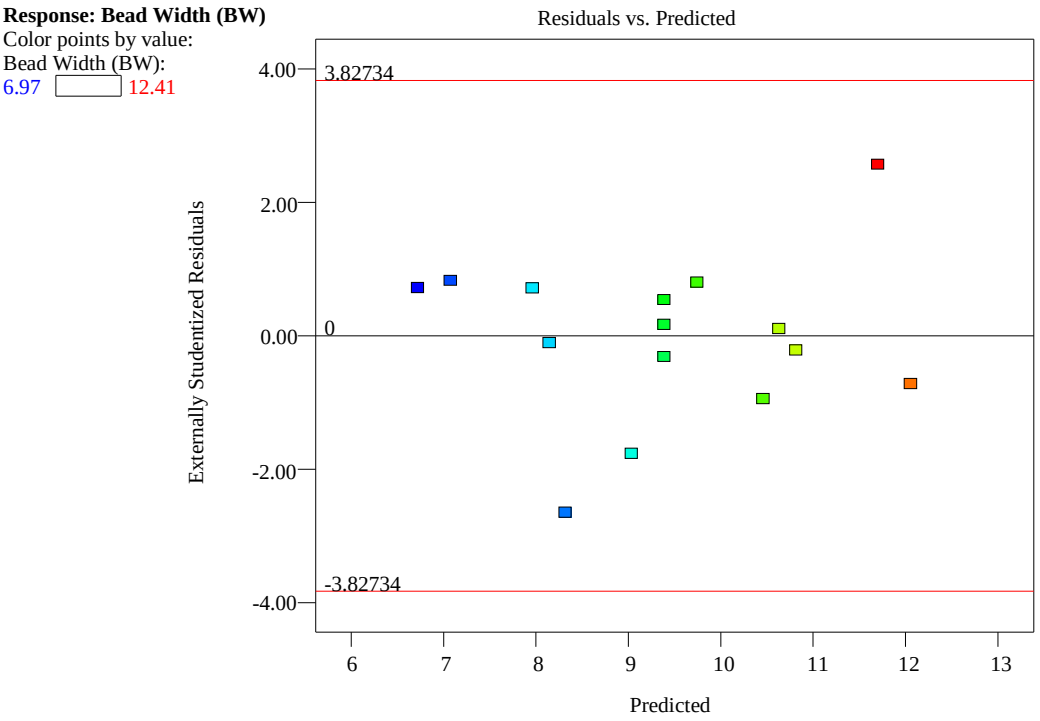

Fig. 21 Plot of externally studentized residuals vs. Predicted for BW

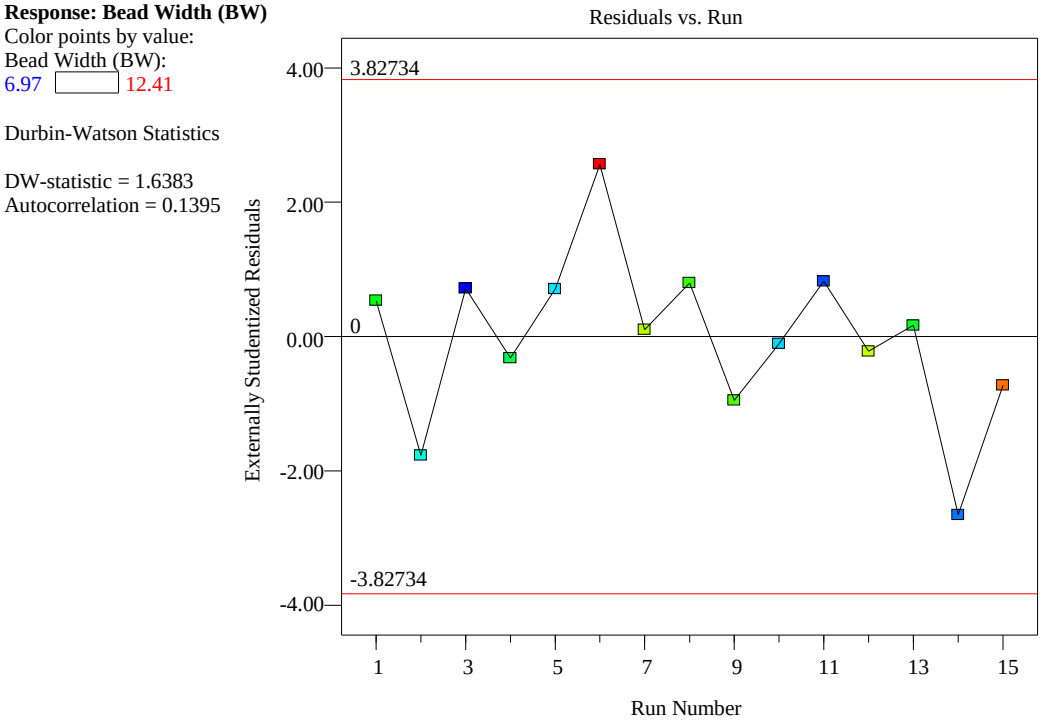

Fig. 22 Plot of externally studentized residuals vs. Run number for BW

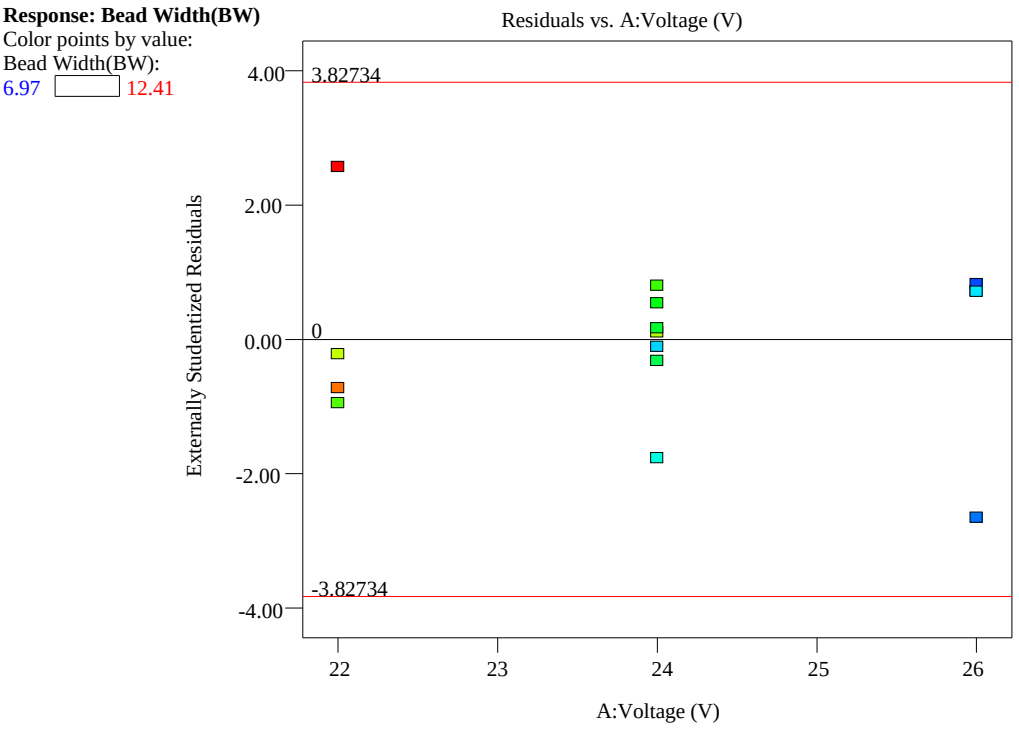

Fig. 23 Plot of externally studentized residuals vs. Input variable – voltage for BW

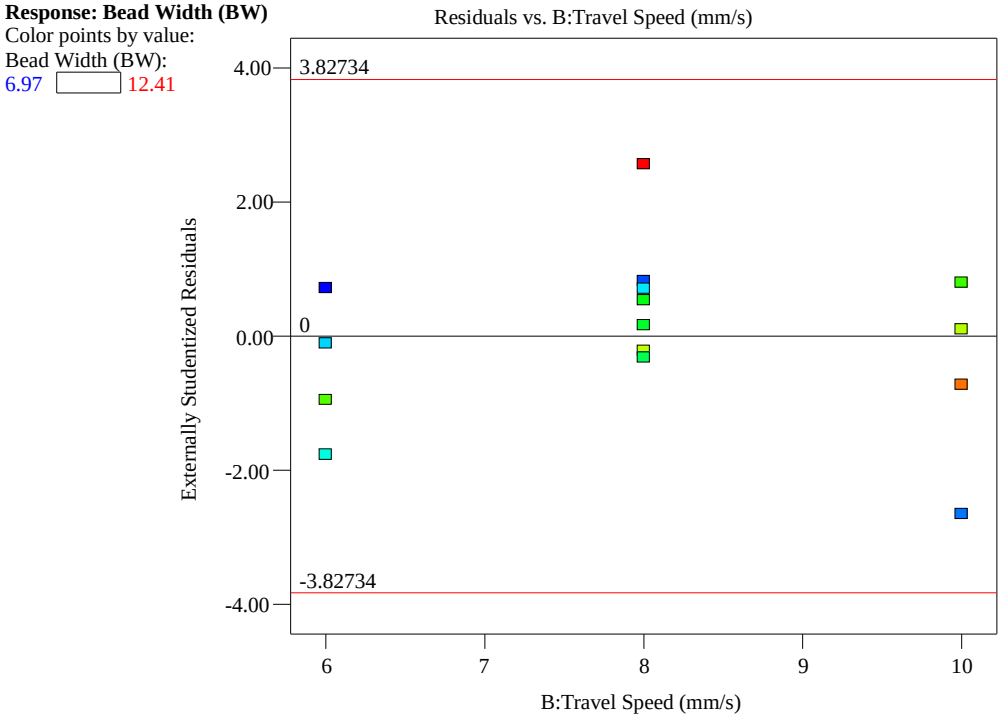

Fig. 24 Plot of externally studentized residuals vs. Input variable – travel speed for BW

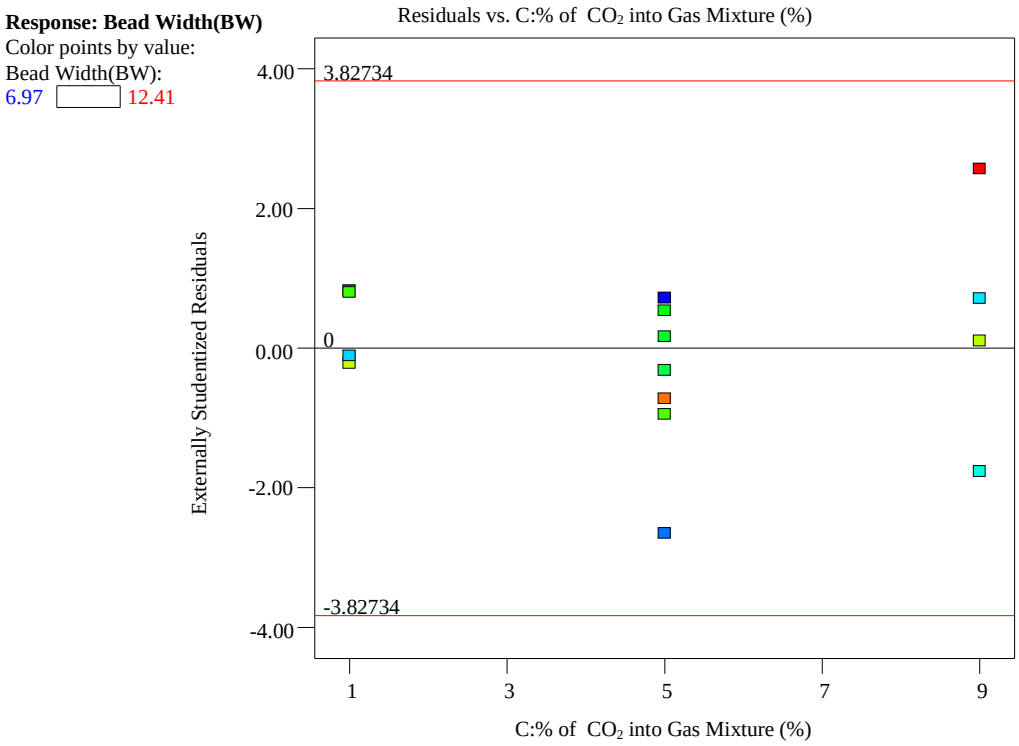

Fig. 25 Plot of externally studentized residuals vs. Input variable – % of CO_2 into the gas mixture for BW

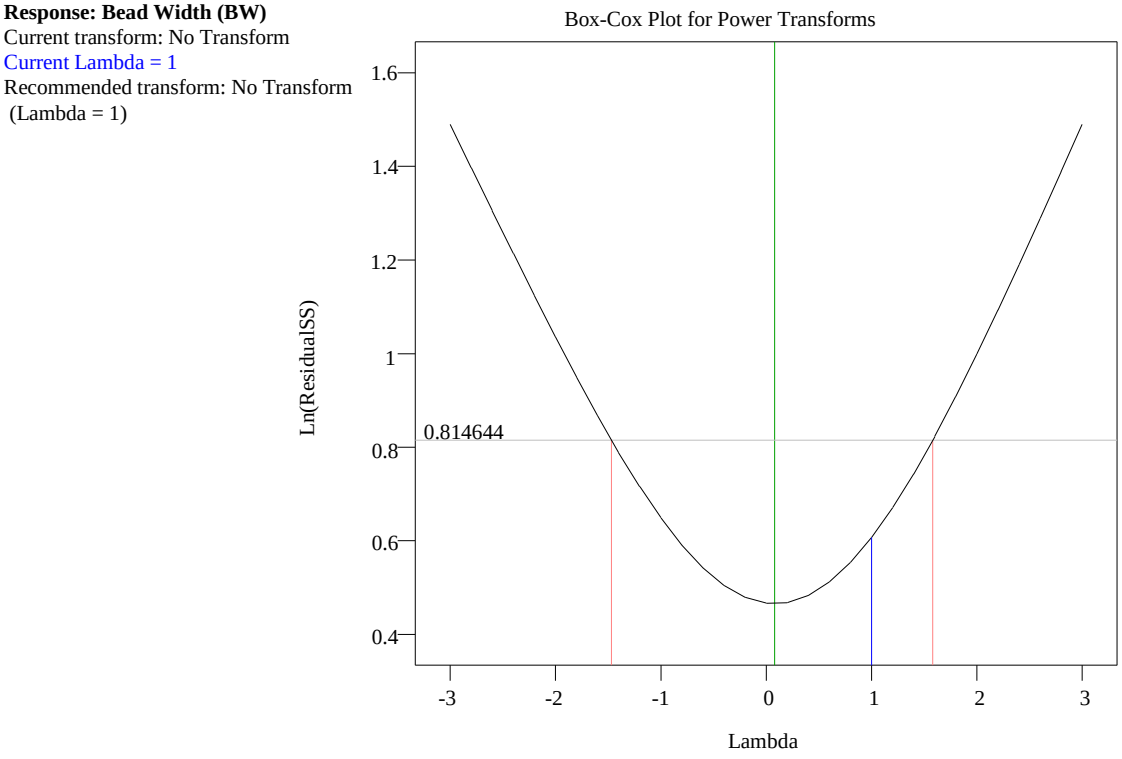

Fig. 26 Box-cox plot for BW

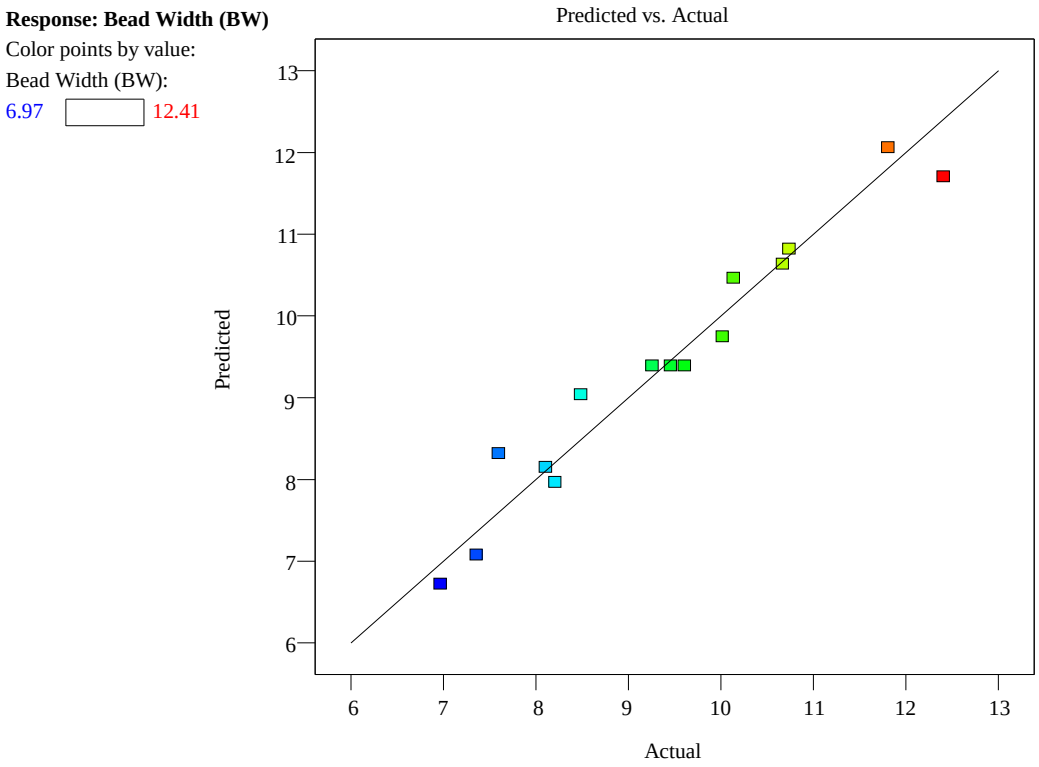

Fig. 27 Externally studentized residuals plot – predicted vs. Actual for BW

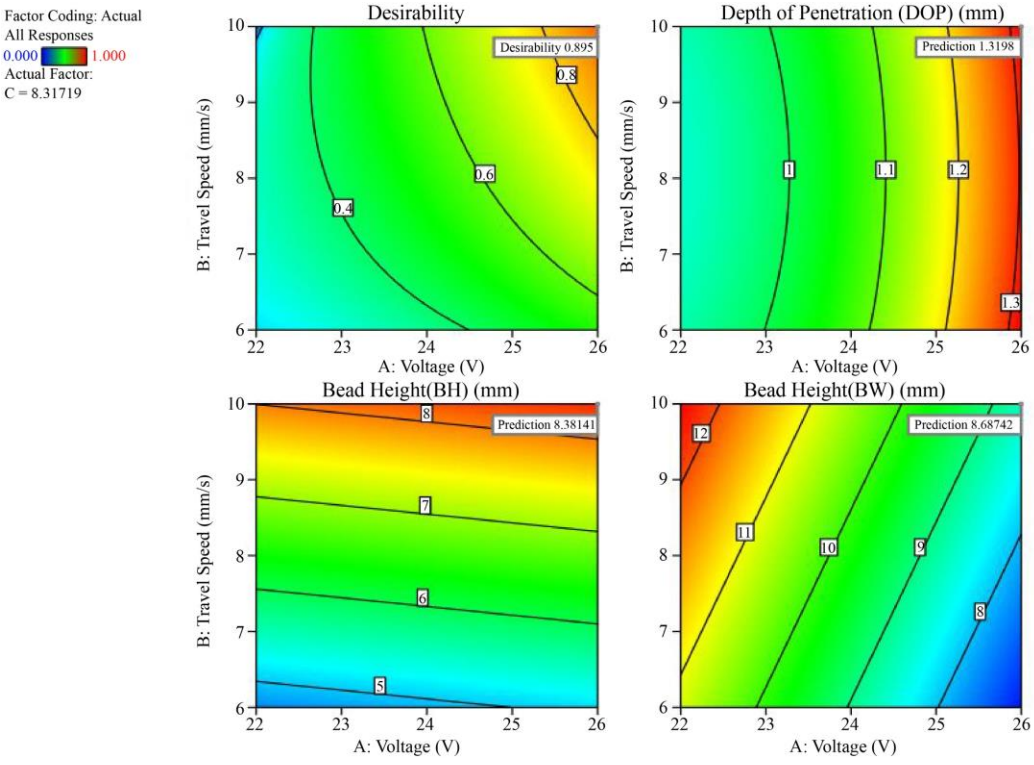

Fig. 28 Contour plot of desirability, DOP, BH, and BW for voltage vs. Travel speed

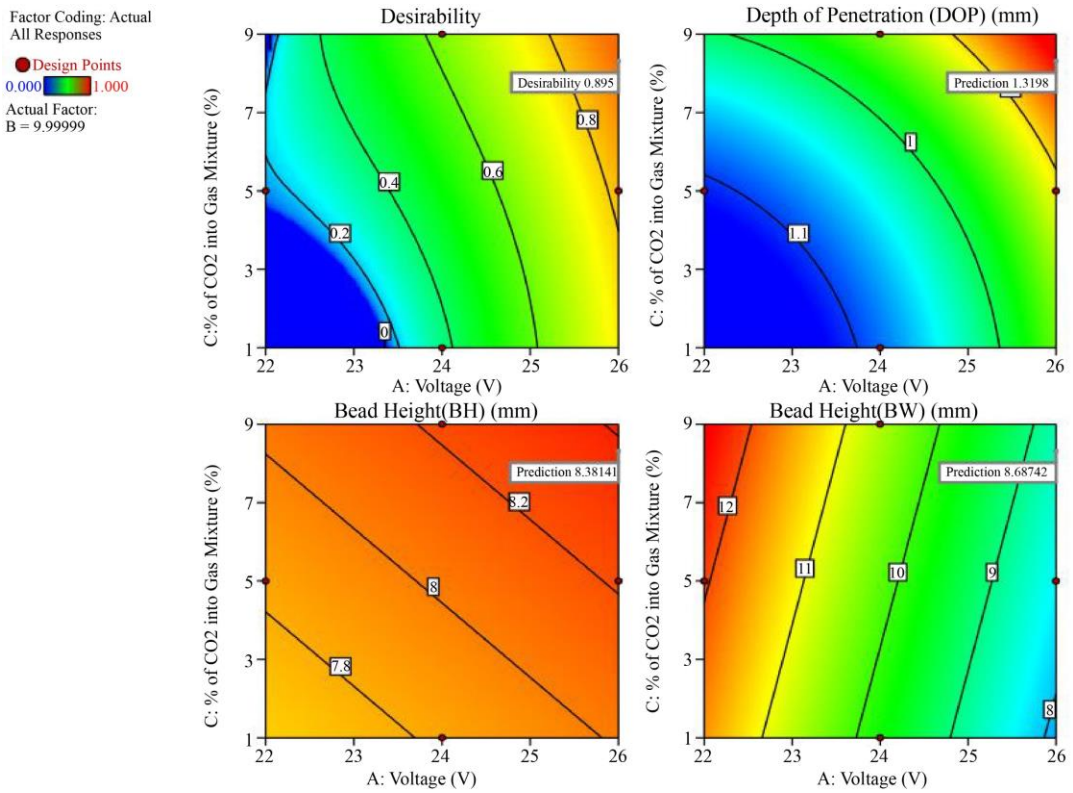

Fig. 29 Contour plot of desirability, DOP, BH, and BW for voltage vs. % of CO_2 into the gas mixture

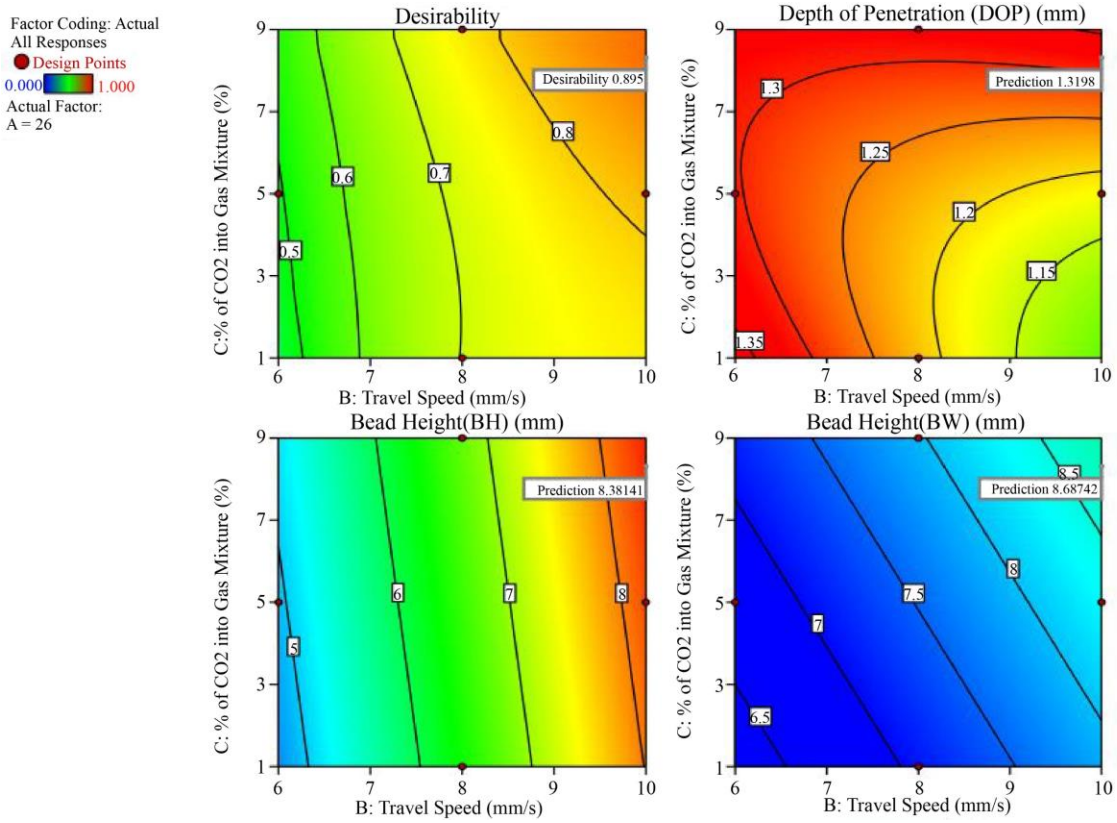

Fig. 30 Contour plot of desirability, DOP, BH, and BW for travel speed vs. % of CO_2 into the gas mixture

Table 8. Outcomes for the various input parameters using state ease 360 software

Sr. No.	Voltage (V)	Travel Speed (mm/s)	% of CO_2 into the Gas Mixture	DOP (mm)	BH (mm)	BW (mm)	Desirability	
1	26.000	10.000	8.317	1.320	8.381	8.687	0.895	Selected
2	26.000	10.000	8.317	1.320	8.381	8.687	0.895	
3	26.000	10.000	8.346	1.321	8.383	8.691	0.895	
4	26.000	10.000	8.347	1.321	8.383	8.691	0.895	
5	26.000	10.000	8.350	1.322	8.383	8.691	0.895	
6	26.000	10.000	8.374	1.323	8.384	8.694	0.895	
7	26.000	10.000	8.376	1.323	8.384	8.694	0.895	
8	26.000	10.000	8.375	1.323	8.384	8.694	0.895	
9	26.000	10.000	8.381	1.323	8.385	8.695	0.895	
10	26.000	10.000	8.383	1.323	8.385	8.695	0.895	
11	26.000	10.000	8.385	1.323	8.385	8.695	0.895	
12	26.000	10.000	8.404	1.324	8.386	8.697	0.895	
13	26.000	10.000	8.410	1.325	8.386	8.698	0.895	
14	26.000	10.000	8.415	1.325	8.386	8.698	0.895	
15	26.000	10.000	8.433	1.326	8.387	8.700	0.895	
16	26.000	10.000	8.442	1.326	8.388	8.701	0.895	
17	26.000	10.000	8.461	1.327	8.389	8.703	0.895	
18	26.000	10.000	8.471	1.328	8.389	8.704	0.895	
19	26.000	10.000	8.492	1.329	8.390	8.707	0.895	
20	26.000	10.000	8.499	1.329	8.390	8.708	0.895	
21	26.000	10.000	8.528	1.331	8.392	8.711	0.894	
22	26.000	10.000	8.557	1.332	8.393	8.714	0.894	
23	26.000	10.000	8.585	1.334	8.395	8.717	0.894	
24	25.999	10.000	8.556	1.332	8.393	8.715	0.894	
25	26.000	10.000	8.597	1.334	8.395	8.718	0.894	
26	26.000	9.986	8.323	1.320	8.370	8.682	0.894	
27	26.000	10.000	8.609	1.335	8.396	8.720	0.894	
28	26.000	9.986	8.323	1.320	8.370	8.683	0.894	
29	26.000	10.000	8.289	1.318	8.380	8.684	0.894	
30	26.000	10.000	8.638	1.337	8.397	8.723	0.894	
31	26.000	10.000	8.642	1.337	8.398	8.723	0.894	
32	26.000	10.000	8.650	1.337	8.398	8.724	0.894	
33	26.000	9.985	8.362	1.322	8.372	8.687	0.894	
34	26.000	10.000	8.667	1.338	8.399	8.726	0.894	
35	26.000	10.000	8.696	1.340	8.400	8.729	0.894	
36	26.000	10.000	8.699	1.340	8.400	8.730	0.894	
37	26.000	10.000	8.695	1.340	8.400	8.730	0.894	
38	26.000	9.985	8.421	1.325	8.374	8.693	0.894	
39	26.000	9.984	8.407	1.324	8.373	8.691	0.894	
40	26.000	10.000	8.724	1.341	8.402	8.733	0.894	
41	25.986	10.000	8.359	1.320	8.382	8.705	0.894	
42	26.000	10.000	8.277	1.318	8.379	8.683	0.894	
43	26.000	10.000	8.745	1.342	8.403	8.735	0.894	
44	26.000	10.000	8.754	1.343	8.403	8.736	0.894	
45	26.000	10.000	8.771	1.344	8.404	8.738	0.894	
46	26.000	10.000	8.784	1.344	8.405	8.739	0.894	
47	26.000	10.000	8.800	1.345	8.405	8.741	0.894	
48	25.985	10.000	8.411	1.322	8.385	8.712	0.894	
49	26.000	10.000	8.828	1.347	8.407	8.744	0.894	
50	25.986	10.000	8.447	1.324	8.386	8.715	0.894	
51	26.000	10.000	8.858	1.348	8.408	8.747	0.894	

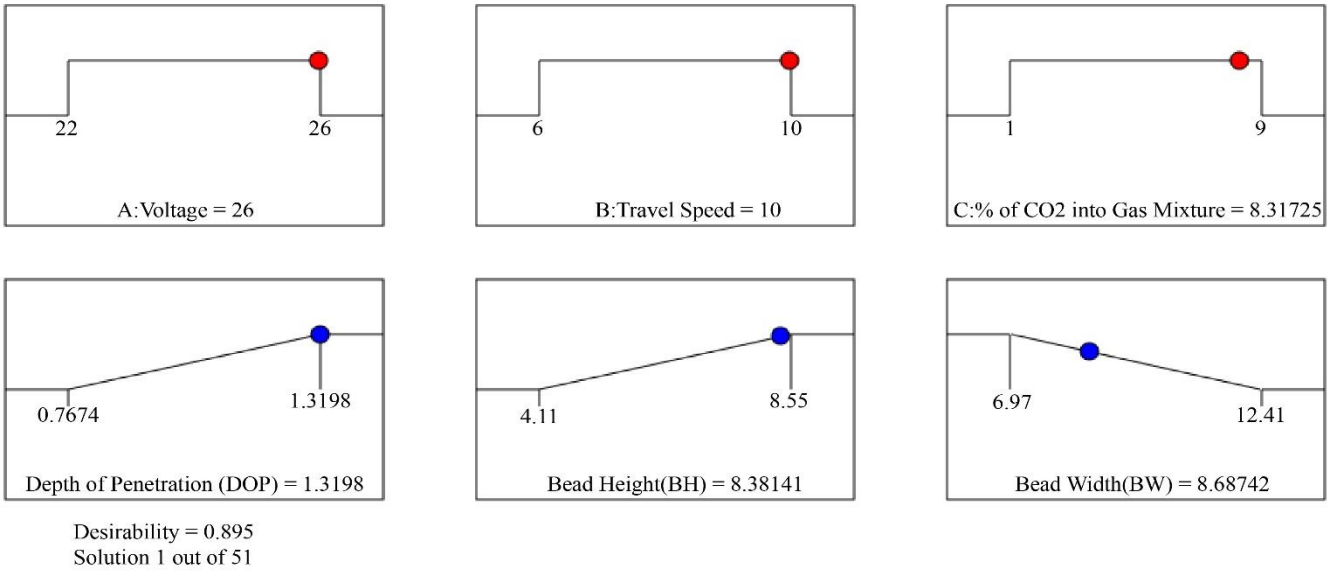

Fig. 31 Ramps graph for the optimum input parameters and optimum outcomes

(a) **(b)**

Fig. 32 Multilayer structure (a) Length, and (b) Width obtained in experimental work for the optimized input parameters.

Table 10. Experimental results

Trial	Voltage (V)	Travel Speed (mm/s)	% of CO_2 into the gas mixture	DOP (mm)	BH (mm)	BW (mm)
1	26	10	8	1.30	8.64	8.54
2	26	10	8	1.37	7.92	7.78
3	26	10	8	1.28	8.66	8.44
4	26	10	8	1.40	8.14	8.74
5	26	10	8	1.35	8.60	8.72

4. Conclusion

Optimizing the process/input parameters to attain the best possible performance of the GMAW-based WAAM process employing Metalloy 80B2 (1.00-1.50 percent chromium and 0.50 percent molybdenum steel), a gas-shielded metal-cored wire, was the main goal of the current study. DOP, BH, and BW of bead deposition made using the GMAW technique of WAAM were examined in relation to the effects of variations in voltage (22 to 26 V), travel speed (1 to 6 mm/s), and shielding gas composition (CO_2 - 1 percent, 5 percent, and 9 percent and Argon - 99 percent, 95 percent, and 91 percent). The BBDs of RSM were used to obtain the optimum combination of input variables (voltage, travel speed, % of CO_2 into gas mixture) using State Ease 360 software for the experimental work. Metalloy 80B2, a gas-shielded metal-cored wire, was employed for bead deposition in single or multiple passes.

The correlation for DOP, BH, and BW was established for the experimental results as a function of input parameters like voltage, speed of travel, and the percentage of CO_2 in the gas mixture. Using ANOVA, the model's and correlation's significance was confirmed. The results of ANOVA indicated that voltage was a more important parameter for the DOP and BW, whereas travel speed is a more important parameter for BH. The F-value and p-value for lack of fit value obtained using ANOVA indicated that predicted correlations were adequate. The fit statistics for DOP, BH, and BW were studied to evaluate the performance of forecasting correlation. From the fit statistics analysis, the difference between the adjusted R2 and predicted R2 value was observed to be less than 0.2, and adequate precision was observed to be higher than 4, indicating that correlation is adequate for predicting response parameters and adequate model discrimination. The various externally studentized residual plots for DOP, BH, and BW were also studied, indicating that developed correlations are valid and no transformation is necessary.

The optimum outcomes from Stat-Ease 360 software: DOP = 1.320 mm, BH = 8.381 mm, BW = 8.687 mm for the input parameter of voltage = 26 V, travel speed = 10 mm/s, % of CO_2 into gas mixture = 8.317% was achieved with the desirability of 0.895. The observations indicate that the average defaults were lower than 6%. The experimental work for the optimum input parameter of voltage = 26 V, travel speed = 10 mm, and % of CO_2 into gas mixture = 8 (due to limitation in setting in an experiment setup) was conducted in five sets. The best result of experimentation was found within the range of ± 5% of results obtained from the State Ease 360 software. The multilayer structure (length and width) obtained from experimentation was bead-on-bead material deposited homogeneously in a multilayer structure, achieved a smooth layer with fusion, and was free from disbanding. The present investigation will be quite useful for manufacturing multilayer structures in industry.

References

[1] Mohsen Attaran, "The Rise of 3-D Printing: The Advantages of Additive Manufacturing Over Traditional Manufacturing," *Business Horizons*, vol. 60, no. 5, pp. 677-688, 2017. [CrossRef] [Google Scholar] [Publisher Link]

[2] Nor Ana Rosli et al., "Review on Effect of Heat Input for Wire Arc Additive Manufacturing Process," *Journal of Materials Research and Technology*, vol. 11, pp. 2127-2145, 2021. [CrossRef] [Google Scholar] [Publisher Link]

[3] Ilbey Karakurt, and Liwei Lin, "3D Printing Technologies: Techniques, Materials, and Post-Processing," *Current Opinion in Chemical Engineering*, vol. 28, pp. 134-143, 2020. [CrossRef] [Google Scholar] [Publisher Link]

[4] Vishal Kumar, Deepti Ranjan Sahu, and Amitava Mandal, "Parametric Study and Optimization of GMAW based AM Process for Multi-layer Bead Deposition," *Materials Today: Proceedings*, vol. 62, pp. 255-261, 2022. [CrossRef] [Google Scholar] [Publisher Link]

[5] Cleber Marques et al., "Analysis of the Solid Wire Dip in the GMAW-CMT Melting Pool as a Means for Enhancing Additive Manufacturing," *Journal of the Brazilian Society of Mechanical Sciences and Engineering*, vol. 45, 2023. [CrossRef] [Google Scholar] [Publisher Link]

[6] Jayaprakash Sharma Panchagnula, and Suryakumar Simhambhatla, "Manufacture of Complex Thin-Walled Metallic Objects using Weld-Deposition based Additive Manufacturing," *Robotics and Computer-Integrated Manufacturing*, vol. 49, pp. 194-203, 2018. [CrossRef] [Google Scholar] [Publisher Link]

[7] Junbiao Shi et al., "Effect of In-Process Active Cooling on Forming Quality and Efficiency of Tandem GMAW–based Additive Manufacturing," *The International Journal of Advanced Manufacturing Technology*, vol. 101, pp. 1349-1356, 2019. [CrossRef] [Google Scholar] [Publisher Link]

[8] Philipp Henckell et al., "In Situ Production of Titanium Aluminides during Wire Arc Additive Manufacturing with Hot-Wire Assisted GMAW Process, *Metals*, vol. 9, no. 5, pp. 1-13, 2019. [CrossRef] [Google Scholar] [Publisher Link]

[9] Philipp Henckell et al., "Reduction of Energy Input in Wire Arc Additive Manufacturing (WAAM) with Gas Metal Arc Welding (GMAW)," *Materials*, vol. 13, no. 11, pp. 1-18, 2020. [CrossRef] [Google Scholar] [Publisher Link]

[10] Ashish Kumar, and Kuntal Maji, "Selection of Process Parameters for Near-Net Shape Deposition in Wire Arc Additive Manufacturing by Genetic Algorithm," *Journal of Materials Engineering and Performance*, vol. 29, pp. 3334-3352, 2020. [CrossRef] [Google Scholar] [Publisher Link]

[11] C.H. Bharat Kumar, and V. Anandakrishnan, "Experimental Investigations on the Effect of Wire Arc Additive Manufacturing Process Parameters on the Layer Geometry of Inconel 825," *Materials Today: Proceedings*, vol. 21, pp. 622-627, 2020. [CrossRef] [Google Scholar] [Publisher Link]

[12] Justin Baby, and Murugaiyan Amirthalingam, "Microstructural Development during Wire Arc additive Manufacturing of Copper-based Components," *Welding in the World*, vol. 64, pp. 395-405, 2020. [CrossRef] [Google Scholar] [Publisher Link]

[13] Adam M. Pringle et al., "Open Source Arc Analyzer: Multi-Sensor Monitoring of Wire Arc Additive Manufacturing," *Hardware*, vol. 8, pp. 1-23, 2020. [CrossRef] [Google Scholar] [Publisher Link]

[14] E. Aldalur, A. Suárez, and F. Veiga, "Metal Transfer Modes for Wire Arc Additive Manufacturing Al-Mg Alloys: Influence of Heat Input in Microstructure and Porosity," *Journal of Materials Processing Technology*, vol. 297, 2021. [CrossRef] [Google Scholar] [Publisher Link]

[15] Wenyong Zhao et al., "Modeling and Simulation of Heat Transfer, Fluid Flow and Geometry Morphology in GMAW-based Wire Arc Additive Manufacturing," *Welding in the World*, vol. 65, pp. 1571-1590, 2021. [CrossRef] [Google Scholar] [Publisher Link]

[16] Rama Kishore Mookara et al., "Influence of Droplet Transfer Behaviour on the Microstructure, Mechanical Properties and Corrosion Resistance of Wire Arc Additively Manufactured Inconel (IN) 625 Components," *Welding in the World*, vol. 65, pp. 573-588, 2021. [CrossRef] [Google Scholar] [Publisher Link]

[17] Reyazul Warsi, and Kashif Hasan Kazmi, and Mukesh Chandra, "Mechanical Properties of Wire and Arc Additive Manufactured Component Deposited by a CNC Controlled GMAW," *Materials Today: Proceedings*, vol. 56, pp. 2818-2825, 2022. [CrossRef] [Google Scholar] [Publisher Link]

[18] Vishal Kumar et al., "Parametric Study and Characterization of Wire arc Additive Manufactured Steel Structures," *The International Journal of Advanced Manufacturing Technology*, vol. 115, pp. 1723-1733, 2021. [CrossRef] [Google Scholar] [Publisher Link]

[19] Teresa Artaza et al., "Wire Arc Additive Manufacturing Ti6al4v Aeronautical Parts using Plasma Arc Welding: Analysis of Heat-Treatment Processes in Different Atmospheres," *Journal of Materials Research and Technology*, vol. 9, no. 6, pp. 15454-15466, 2020. [CrossRef] [Google Scholar] [Publisher Link]

[20] M.J. Bermingham et al., "High Strength Heat-treatable β-titanium Alloy for Additive Manufacturing," *Materials Science and Engineering: A*, vol. 791, 2020. [CrossRef] [Google Scholar] [Publisher Link]

[21] Rui Fu et al., "Large-size Ultra-High Strength-Plasticity Aluminum Alloys Fabricated by Wire arc Additive Manufacturing via Added Nanoparticles," *Materials Science and Engineering: A*, vol. 864, 2023. [CrossRef] [Google Scholar] [Publisher Link]

[22] Maximilian Gierth et al., "Wire Arc Additive Manufacturing (WAAM) of Aluminum Alloy AlMg5Mn with Energy-Reduced Gas Metal Arc Welding (GMAW)," *Materials*, vol. 13, no. 12, pp. 1-22, 2020. [CrossRef] [Google Scholar] [Publisher Link]

[23] Angela Dean, Daniel Voss, and Danel Draguljić, *Response Surface Methodology*, Design and Analysis of Experiments, 2nd ed., Springer Cham, pp. 565-614, 2017. [CrossRef] [Google Scholar] [Publisher Link]

[24] André I. Khuri, and Siuli Mukhopadhyay, "Response Surface Methodology," *WIREs Computational Statistics*, vol. 2, no. 2, pp. 128-149, 2010. [CrossRef] [Google Scholar] [Publisher Link]